CrossMark

ORIGINAL PAPER

Experimental petrology constraints on the recycling of mafic cumulate: a focus on Cr-spinel from the Rum Eastern Layered Intrusion, Scotland

Julien Leuthold[1,2] · Jonathan D. Blundy[1] · Richard A. Brooker[1]

Abstract *Reactive liquid flow* is a common process in layered intrusions and more generally in episodically refilled magma chambers. Interaction between newly injected melt and cumulates, or crystal mushes, perturbs the liquid line of descent of the melt and modifies mineral chemistry and texture. We present insights into the effects of assimilation of mafic cumulate rocks (gabbro, troctolite) by cogenetic Mg-rich basalt liquid using one-atmosphere, controlled $f\mathrm{O_2}$ phase equilibrium experiments on picritic parental liquid to the Rum layered intrusion, Scotland. For picrite-only experiments at $f\mathrm{O_2}$ = QFM, Cr-spinel (Cr# = Cr/[Cr + Al + Fe^{3+}] = 0.43; Fe# = Fe^{2+}/[Mg + Fe^{2+}] = 0.32) saturates at 1320 °C, olivine (Fo$_{88}$) at ~1290 °C, plagioclase (An$_{77}$) at 1200 °C, and clinopyroxene (Mg#: 0.81) at 1180 °C. In melting experiments on picrite + gabbro mixtures, plagioclase (1230 °C, An$_{80}$) and clinopyroxene (1200 °C, Mg#: 0.85) saturation temperature and mode are increased significantly. Cr-spinel in these experiments has a distinctive, low Fe#. In melting experiments on picrite + troctolite mixtures, plagioclase (An$_{86}$) saturates at 1240 °C and clinopyroxene (Mg#: 0.81) at 1170 °C. Al-rich spinel crystallizes at high temperature (>1220 °C) and becomes more Cr-rich upon cooling, reaching the highest Cr# = 0.47 at 1180 °C (0.54 at QFM-1.2).

The experimental results confirm that plagioclase and clinopyroxene stability plays a major role in determining the composition of coexisting spinel. Comparing our experimental results to the Rum Eastern Layered Intrusion, we propose a model for the precipitation of spinel from picrite–troctolite hybrid melt that is compatible with the observed olivine, plagioclase, and clinopyroxene chemistry.

Keywords Rum layered intrusion · Cr-spinel · Gabbro melting · Troctolite melting · Picrite · 1atm experimental petrology · Reactive liquid flow

Communicated by Timothy L. Grove.

✉ Julien Leuthold
julien.leuthold@erdw.ethz.ch

1 School of Earth Sciences, University of Bristol, Wills Memorial Building, Bristol BS8 1RJ, United Kingdom

2 Department of Earth Sciences, ETH Zürich, Clausiusstrasse 25, 8092 Zürich, Switzerland

Introduction

Magma chambers are built up incrementally by repeated injections of melt into a growing crustal reservoir (e.g., Saint Blanquat et al. 2011; Leuthold et al. 2012). In open magmatic systems, successive recharge of hot melt rejuvenates and assimilates resident crystal mush and cumulates (Tronnes 1990; Hildreth and Moorbath 1988; Bédard and Hébert 1998; Dungan and Davidson 2004; Leuthold et al. 2014a, b). This process plays a critical role in the construction of large magma chambers via accumulation of successive sills or dykes (Annen et al. 2006; Solano et al. 2012) and is responsible for the modification of percolating melt composition and cumulate/crystal mush mineral chemistry, texture, and abundance. Interaction between resident cumulate mush and newly injected liquid (*reactive liquid flow*, or *infiltration metasomatism*, as defined by Irvine 1980) modifies both the cumulate and the reactive liquid, changing their modal composition, chemistry, and texture (Fig. 1) (Leuthold et al. 2014a). O'Hara and Herzberg (2002) stated that despite its importance, the assimilation of mafic crystals/cumulates by mafic melts is frequently underestimated.
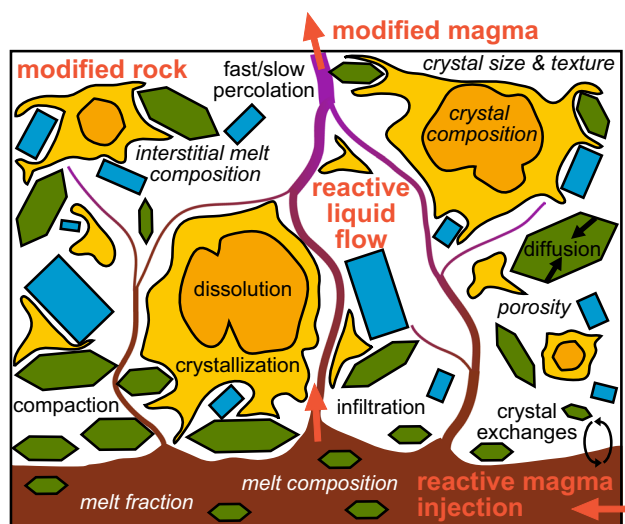
Fig. 1 Schematic representation of the complex *reactive liquid flow* process (modified from Leuthold et al. 2014a). Percolation of reactive liquid within crystal mush has important consequences: Crystal chemistry and textures are modified by dissolution–recrystallization and re-equilibration; the rock structure is changed by compaction and modification of the mineral mode; the crystals chemistry is modified by diffusion; and the percolating liquid chemistry is changed by assimilation, mixing and mingling, perturbing the normal liquid line of descent

The lack of mineralogical, chemical, and isotopic contrast between reactants can make it difficult to detect and distinguish crystal–melt interaction from simple crystallization. Nevertheless, modifications of mineral chemistry and texture and melt composition have been revealed by detailed studies of intrusive rocks in a variety of geodynamic settings (e.g., Hildreth and Moorbath 1988; Bédard and Hébert 1998; Leuthold et al. 2014a, b).

In this study, we will examine the consequences of *reactive liquid flow* on the newly injected hot liquid whose composition is modified by assimilation of cogenetic mafic crystal mush and cumulate (troctolite, gabbro). We show that this has important consequences for the phase equilibria and chemistry, particularly spinel compositions. Spinels crystallize down temperature from the liquidus for a wide range of mafic magmas, in different tectonic environments (Roeder 1994). Understanding Cr-spinel (chromite) petrogenesis is of particular importance in layered intrusions, where chromitites are associated with platinum group element (PGE) ore deposits (e.g., Power et al. 2000; Grieco et al. 2004; O'Driscoll et al. 2009a, Latypov et al. 2013). Chromitite formation has long been debated, and several petrogenetic models exist (see Campbell and Murck 1993; Naldrett et al. 2012), including liquid immiscibility (McDonald 1965), oxidation (Ulmer 1969; Cameron and Desborough 1969), pressure fluctuations (Lipin 1993), and assimilation of silicic crustal rock by mafic magma (Irvine 1975; Spandler et al. 2005). Studying ophiolites, Bédard

and Hébert (1998) have demonstrated the formation of chromitite via assimilation of crustal pyroxenite and gabbro by picrite melt intrusion. However, the most widely accepted model involves Cr-spinel saturation by mixing and hybridization of a newly injected olivine-saturated magma with a cogenetic, differentiated, more siliceous melt (Irvine 1977).

We will use the Rum Eastern Layered Intrusion (Scotland) as a case study. This shallow, open-system, layered intrusion shows some of the world's best examples of *reactive liquid flow* (Leuthold et al. 2014a). The hybridization model of Irvine (1977) was applied to the Rum Eastern Layered Intrusion chromitites layers by Young (1984). O'Driscoll et al. (2009b) proposed an alternative model for the same chromitite occurrences on Rum whereby new picritic liquid assimilated troctolite cumulate. We will run a series of experiments to test the effect of gabbro and troctolite assimilation on the picrite liquid line of descent. We have chosen to run our experiments at atmospheric pressure (0.1 MPa) because of the ease of controlling oxygen fugacity, a key magmatic variable, in a gas-mixing furnaces and the very low emplacement pressure of the Rum Eastern Layered Intrusion. The present experiments allow us to evaluate different hypotheses regarding the origin of chromitites on Rum, but with application to other layered intrusions and spreading ridges.

The Rum Eastern Layered Intrusion

The Paleogene Rum Igneous Complex is part of the British Tertiary Volcanic Province and the North Atlantic Igneous Province (Emeleus and Gyopari 1992; Bell and Williamson 2002), dated at 60.53 ± 0.08 Ma by Hamilton et al. (1998), and related to the proto-Iceland plume (Kent 1995; Saunders et al. 1997; Bell and Williamson 2002). The Complex was intruded along the unconformity between the Archaean Lewisian gneiss and the overlying Precambrian arkoses of the Torridonian Group, at a pressure of 15 ± 5 MPa (Holness 1999). It is a bimodal intrusive complex with an initial episode of felsic activity and subsequent emplacement of a layered ultramafic to mafic braided sill complex (Leuthold et al. 2014b) into a caldera (Emeleus 1997). Successive replenishments by mafic magma have built alternating olivine-rich and plagioclase-rich cumulate layers (Appendix figure 1). The Eastern Layered Intrusion is composed of a 750-m-thick cumulate pile, divided into 15 intrusive units (Appendix figure 2). Each unit is formed of *peridotite* (olivine-rich cumulate) overlain by plagioclase-bearing cumulate (troctolite, gabbro, and poikilitic gabbro, in variable proportions known collectively as *allivalite*). The sill complex was fed by new magma

Table 1 Composition of starting materials (wt %)

	Picrite B62/2[a]	Basalt 11JL33[b]	Troctolite 11JL16[b]	Gabbro 11JL27[b]
SiO_2	45.76	47.09	42.93	48.66
TiO_2	1.56	2.14	0.08	0.29
Al_2O_3	13.58	14.12	18.03	16.30
Cr_2O_3	0.11	0.03	0.09	0.10
Fe_2O_3	12.38	13.21	8.26	6.26
MnO	0.19	0.2	0.11	0.11
MgO	12.42	6.47	19.44	10.83
CaO	11.25	10.43	9.79	15.39
NiO	0.04	0.01	0.07	0.03
Na_2O	2.23	2.97	0.62	1.31
K_2O	0.16	0.57	0.02	0.02
P_2O_5	0.13	0.20	0.01	0.01
LOI	0.51	2.58	0.27	0.61
Total	100.32	100.04	99.72	99.92
Mg#[c]	0.67	0.49	0.82	0.77

Composition of the Rum B62/2 picritic dyke (Upton et al. 2002), 11JL27 gabbro, and 11JL16 troctolite (Leuthold et al. 2014a) that were mixed in different proportions to make the starting materials of our experiments

[a] Upton et al. (2002)

[b] Leuthold et al. (2014a)

[c] Molar Mg#

injections along the Central Zone fault originating from a magma source at a depth of several kilometers (Emeleus et al. 1996). The intrusive units were thought originally to have formed by fractionation of individual batches of olivine–phyric picrite melts (Brown 1956; Upton et al. 2002). Later studies showed that many units are composite and formed from successive, relatively small batches of either picritic or basaltic magma (Renner and Palacz 1987; Bédard et al. 1988; Holness and Winpenny 2009). The cumulates themselves were later intruded by picritic magma (Bédard et al. 1988). Thus, the Rum Eastern Layered Intrusion is an excellent example of *reactive liquid flow processes* (Fig. 1) in an open magmatic system. Some of the best evidences of partial melting of resident troctolite and gabbro rocks by intrusive picrite liquids and subsequent melt hybridization include Cr-spinel-bearing anorthosite produced after picrite percolation through troctolite (O'Driscoll et al. 2009b, 2010); formation of poikilitic gabbro with clinopyroxene oikocrysts (ca. 1 cm across) formed in gabbro percolated by hybrid melt (Leuthold et al. 2014a); and bulk rock reversals in isotopic composition (Palacz and Tait 1985). Some troctolite and peridotite might also be the products of such modifications, representing highly reacted cumulates (Leuthold et al. 2014a).

Methods

Starting materials

Starting materials consisted of finely ground rock powders from four samples of the Rum Eastern Layered Intrusion (Table 1): a near-primary olivine–phyric picritic dyke (B62/2; McClurg 1982, unpublished PhD. thesis; Upton et al. 2002), a basaltic dyke (11JL33; Leuthold et al. 2014a), a gabbro (11JL27; Leuthold et al. 2014a), and a troctolite (11JL16, Leuthold et al. 2014a). B62/2 contains euhedral to subhedral olivine phenocrysts (~10 vol%, $Fo_{85.9-80.5}$) in a fine-grained matrix composed of granular olivine (Fo_{78-75}) + plagioclase (An_{69-66}) + clinopyroxene (Mg#[1] = 0.82–0.71) + magnetite, with minor amounts of amphibole, mica, and Cr-spinel (Cr#[2] = 0.32–0.43). B62/2 has a mildly alkalic, high MgO (Mg#: 0.67) composition that is a close match to the inferred Rum parental liquid (Upton et al. 2002). B62/2 is thought to have originated from low-degree partial melting of a lherzolite source close to the garnet–spinel transition within the proto-Icelandic mantle plume, with minor subsequent crustal contamination. Recent Icelandic picrites have a similar composition to B62/2 (Hémond et al. 1993). Basaltic dyke starting material 11JL33 has a composition (Mg#: 0.51) very similar to those studied by Toplis and Carroll (1995) and Thy et al. (2006) in the context of the liquid line of descent of the Skaergaard layered intrusion (Greenland). 11JL33 is composed of normally zoned plagioclase (An_{61-15}), clinopyroxene (Mg# = 0.73 to 0.65), K-feldspar, magnetite with ilmenite exsolution (3 vol%), titanite, zircon, epidote, and chlorite. According to McClurg (1982, unpublished PhD. Thesis) and Upton et al. (2002), B62/2 picrite and 11JL33 basalt represent coexisting mafic end-member liquid compositions (Fig. 2). A few picritic dykes at Rum (e.g., M9) have accumulated olivine and spinel macrocrysts crystallized in a near-Moho reservoir (Upton et al. 2002); these deeper intrusions were not considered experimentally but are discussed in terms of petrogenesis.

Partial melts of troctolite and gabbro coexisted with intrusive picrite (Leuthold et al. 2014a). To study experimentally the effect of mafic crystal assimilation into picrite, we used as starting material mechanical mixtures (hybrids) of picrite (B62/2) with gabbro (11JL27) and troctolite (11JL16). Gabbro 11JL27 is composed of 13 vol% olivine, 53 vol% plagioclase, and 34 vol% clinopyroxene. Troctolite 11JL16 is composed of 26 vol% olivine, 0.2 vol% Cr-spinel, 70 vol% plagioclase, and 4 vol% clinopyroxene (see Leuthold et al. 2014a for details). The hybrid series of

---

[1] Mg# = molar Mg/[Mg + Fe^{2+} + Fe^{3+}].

[2] Cr# = molar Cr/[Cr + Al + Fe^{3+}].
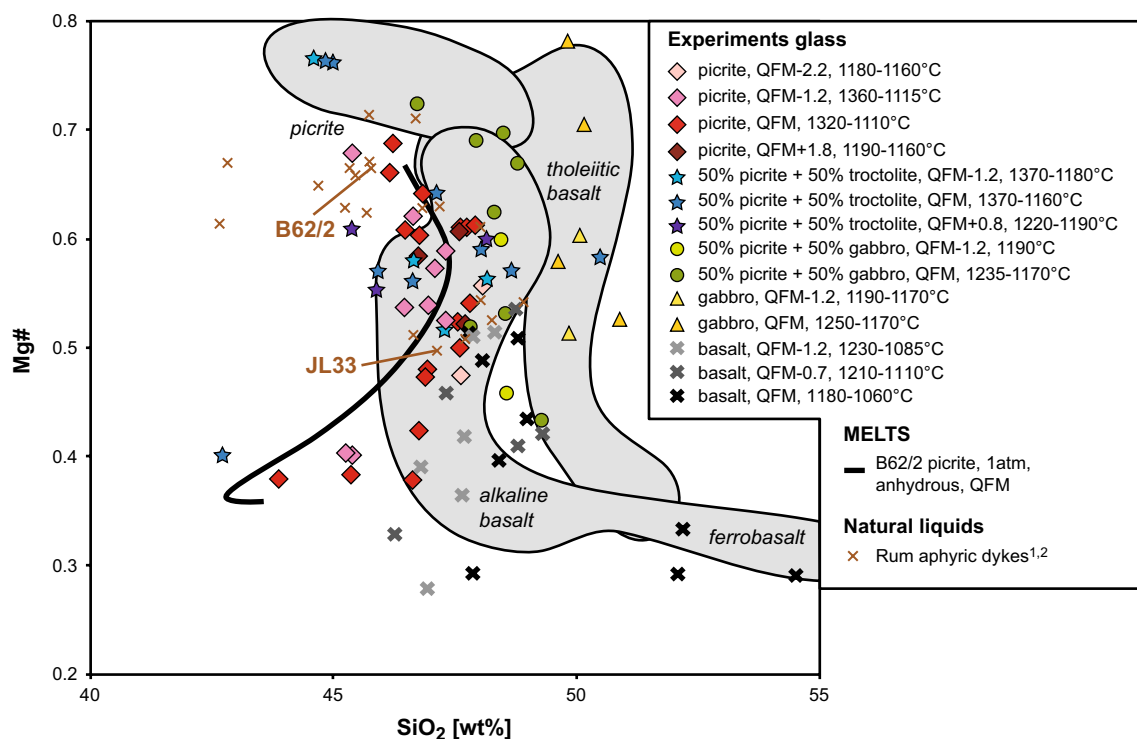
Fig. 2 Experimentally determined liquid compositions. Picrite 1 atm, anhydrous, QFM; MELTS (Ghiorso and Sack 1995; Asimow and Ghiorso 1998) calculations and Rum aphyric dykes are shown for reference (MELTS calculations under reduced conditions [not shown] show a strong final SiO$_2$ increase). B62/2 picrite and 11JL33 basalt were used as starting material in the experiments. Gray areas delimit the composition of Iceland plume mafic lavas (Hémond et al. 1993).

The Rum picrite liquid line of descent is very similar to the trend defined by the Rum dykes and Icelandic alkaline basalt. Through clinopyroxene-rich cumulate assimilation, the experimental glass SiO$_2$ content is distinctly increased. Through clinopyroxene- and/ or olivine-rich cumulate assimilation, the liquid Mg# is increased. [1] McClurg (1982) unpublished PhD thesis, [2] Leuthold et al. (2014a)

experiments is intended to evaluate the effect of variable proportions of mafic rock assimilation (0, 50, and 100 %) on the reactive picrite liquid line of descent.

Experiments

Experiments #27 to #109 were performed at the University of Bristol in GERO™ vertical furnaces at atmospheric pressure. We controlled the oxygen fugacity (fO$_2$) by employing mixed CO and CO$_2$ gases controlled by Alicat Scientific flow controllers. The fO$_2$ was measured before and after each experiment with SIRO2™ solid zirconia oxygen sensors. The temperature was monitored adjacent to the sample with a type B thermocouple. Additional experiments (#110 to #173) were run at ETH, Zurich, using a similar GERO™ vertical furnace with controlled fO$_2$ conditions by mixing CO$_2$ and H$_2$. Results from the two laboratories are mutually consistent.

The starting material powder was mixed with a small amount of ultrapure water, as a binder, and mounted on a thin Pt–Rh wire loop. Most individual mounts were initially melted at supraliquidus conditions and then quenched to a glass. In isothermal experiments, the crystal-free glass was

taken directly to the desired temperature at fO$_2$ of QFM-2.2 to QFM + 1.8[3] (see Appendix figure 2). In cooling rate experiments, different cooling modes were used. In these experiments, we progressively ramped the temperature (<100 °C/h), while adjusting fO$_2$. This method is very similar to that used by Fisk and Bence (1980). In both cases, we also used the temperature oscillation (±10 °C) technique (Mills et al. 2011; Mills and Glazner 2013) to grow coarse crystals. Following ramped cooling, the sample was left to equilibrate typically for 5–15 h and then drop-quenched into water. Crystals show no evidence of quench overgrowths, and the quenched liquid is pure glass. High spatial-resolution core–rim chemical profiles show no rim zoning between crystal pairs or with liquid. These observations are considered to indicate both equilibrium and effective quenching without re-equilibration or recrystallization (e.g., Sisson and Grove 1993b). For comparison with fully molten starting material, we have also run a few melting experiments, where the starting material was equilibrated at a temperature below the liquidus. Additionally, we have also reacted picrite with

---

[3] QFM: Quartz–fayalite–magnetite equilibrium, corresponding to Ni-NiO-0.8 (NNO-0.8).

troctolite. Samples were melted above the liquidus, quenched, and equilibrated at 1250 and 1220 °C at QFM-1.2 prior to juxtaposition and reaction for 2–18 h. Experimental run conditions and products are given in Tables 2, 3, 4, and 5; schematic cooling paths are presented in Appendix figure 2; selected BSE images are shown in Fig. 3; and mineral stability fields are presented in Fig. 4.

Analyses

Run products were mounted in EPOFIX™ resin blocks and polished to 1 μm. We used the University of Bristol Hitachi S-3500N and the ETH Zürich Jeol JSM-6390 LA scanning electron microscopes (SEM), both equipped with Thermo Fisher Noran energy-dispersive spectrometer (EDS X-ray detector), to acquire backscatter electron (BSE) images and characteristic X-ray maps at 20 kV that were used to determine phase assemblages and proportions using *imageJ* software. Repeated analyses on the same samples provided an estimate of the uncertainties on mineral proportions, which were typically less than ±5 vol%. The Bristol JEOL 8530F FEG-EMPA operating at low voltage was required to measure accurately the major element composition of small phases, without contamination by fluorescence from the surrounding glass (Saunders et al. 2014). The operating conditions were 10 kV, 10 nA, and a beam size of 0.1 μm for crystals (spinel has a typical diameter of ~2 μm) and 5–10 μm for glass. Additional analyses were acquired at ETH Zürich, using a JEOL JXA-8200 EMPA, at 15 kV and 20 nA and a beam size of 1 μm for crystals and 5–10 μm for glass. Natural and synthetic silicates and oxides were used as primary and secondary standards. The EMP analyses of the Pt-13Rh wire showed very limited Fe gain during short experiments (<1 h) at high temperature (1260 °C). After an extreme run duration of 60 h at 1170 °C and QFM conditions, the glass once remolten above the liquidus had only lost 1 wt.% FeO_{tot} (10 % relative). The glass Fe^{3+}/Fe_{tot} ratio was calculated using Kress and Carmichael (1991) algorithm at the experimental temperature and fO_2. Glass compositions in fully molten and subsequently re-equilibrated experiments and in partially molten powder are identical, but crystals are strongly zoned in the later and difficult to interpret. Thus, we have decided to focus on the results from fully molten starting materials. Analytical results are presented in Appendix Table 1.

Liquid line of descent

Phase proportions and compositions

The mineral modes are given in Tables 2, 3, 4, and 5 and Fig. 5; mineral compositions are given in Appendix table 1 and Fig. 6. From 1160 °C, the crystals form a connected framework in picrite experiments (46 vol% liquid).

Picritic dyke B62/2, considered as the most probable parental liquid for Rum (Leuthold et al. 2014a), has liquidus and solidus temperatures of 1320 and 1110 °C, respectively (Fig. 4). Olivine and Cr-spinel are the liquidus phases, and plagioclase saturates at 1200 °C and clinopyroxene at 1180 °C (Fig. 4 and Appendix figure 3). The liquid fraction strongly decreases once plagioclase and clinopyroxene saturate (Fig. 5). Upon cooling, the B62/2 experimental glasses become basaltic and finally basanitic (Fig. 2). Their compositions are identical to Iceland plume lavas (Hémond et al. 1993) (Fig. 2). As expected, the olivine forsterite content is higher under more oxidized conditions.

Basalt 11JL33, which is similar in composition to other basaltic dykes on Rum (McClurg 1982, unpublished PhD thesis) has a liquidus temperature of 1165 °C, when olivine, spinel, and plagioclase co-saturate (Figs. 4, 5 and Appendix figure 3). The 11JL33 experiments corroborate the Toplis and Carroll (1995) and Thy et al. (2006) experiments with comparable saturation temperatures and modes for olivine, plagioclase, and clinopyroxene.

Gabbro assimilation by picrite tends to reduce the liquidus and increase the solidus temperatures (Figs. 4, 5). Olivine saturation is delayed in comparison with the picrite starting material and is modally less important, resulting in a higher Mg# at high melt fractions (Figs. 2, 6), amplified by the low liquid FeO content. The glass is CaO- and Al_2O_3-enriched which increases plagioclase and clinopyroxene saturation temperatures (Figs. 2, 4 and Appendix figure 3).

Troctolite assimilation increases the liquidus and solidus temperatures of picrite (Figs. 4, 5), as well as the glass Al_2O_3 and MgO contents. The plagioclase, olivine, and spinel saturation temperatures are all increased, while clinopyroxene stability is decreased (Figs. 4, 5).

Spinel

Crystals are typically euhedral and ~2 μm across. Only spinel in contact with glass was considered to guarantee equilibration with melt during cooling rate experiments. Cr-spinel Fe–Mg re-equilibration with melt is relatively rapid (Scowen et al. 1991); nevertheless, core and rim analyses obtained by the FEG-EMPA reveal the absence of any zoning that may be related to quenching. B62/2 picrite high-temperature QFM crystals (1280 °C), co-crystallizing with olivine, are Cr-rich (Cr# = 0.43, Al/(Al + Cr) = 0.53). From 1230–1200 to 1150 °C, the spinel Al/(Al + Cr) progressively decreases from 0.65 to 0.54 (Fig. 7a). Upon further cooling along the QFM equilibrium, the Fe^{3+} content strongly increases. At and below 1140 °C, Fe enrichment rapidly increases and magnetite becomes the stable spinel phase. Crystals in cooling rate experiments have slightly

Table 2 Gas mixing furnace experiments (1 atm, anhydrous) and run products

Run#	Starting material conditions			Cooling mode	Final equilibration conditions			Phases identified and proportions				
	T (°C)	fO₂	Duration (min)		T (°C)	fO₂	Duration (h)	Liq (%)	Ol (%)	Cr-spl (%)	Plg (%)	Cpx (%)
Experiments with B62/2 picrite												
61	1290	QFM	30	Quenching	1180	QFM-2.2	5.5	x	x	<0.1	x	–
57	1290	QFM	30	Quenching	1160	QFM-2.2	10.0	34	x	–	x	x
174	1330	QFM-1.2	20		1360	QFM-1.2	0.4	100	–	–	–	–
135	1330	QFM-1.2	20	Quenching	1240	QFM-1.2	2.5	90	10	0.1	–	–
136	1330	QFM-1.2	20	Quenching, T oscillation	1200	QFM-1.2	3.5	x	x	x	–	–
137	1340	QFM-1.2	20	Quenching, T oscillation	1190	QFM-1.2	3.3	83	11	0.2	6	–
161	1360	QFM-1.2	20	Quenching, T oscillation	1175	QFM-1.2	6.5	x	x	x	x	x
114/1	1365	QFM	60	Quenching, cooling from 1250 °C, T oscillation	1165	QFM-1.2	69.0	61	11	<0.1	20	8
163	1360	QFM-1.2	20	Quenching, T oscillation	1140	QFM-1.2	17.3	x	x	–	x	x
152	1350	QFM-1.2	20	Quenching, cooling from 1190 °C with T oscillation	1125	QFM-1.2	17.3	27	13	0.1	36	24
28					1320	QFM	0.5	100	–	–	–	–
98	1355	QFM	60	Quenching	1280	QFM	9.5	97	3	x	–	–
62	1290	QFM	30	Quenching	1260	QFM	1.0	96	4	0.1	–	–
60	1260	QFM	30	Quenching, equilibration at 1170 °C (60 h, QFM), melting at 1260 °C	1260	QFM	0.5	x	x	x	–	–
107	1355	QFM	60	Quenching	1230	QFM	5.0	x	x	x	–	–
106	1335	QFM	60	Quenching	1210	QFM	8.3	x	x	x	–	–
87	1310	QFM	30	Quenching	1210	QFM	11.3	x	x	x	–	–
47	1260	QFM	45	Quenching	1210	QFM	7.0	90	9	x	1	–
48	1260	QFM	45	Quenching	1200	QFM	16.3	95	4	0.1	–	–
49	1260	QFM	60	Cooling	1190	QFM	8.3	89	11	0.2	–	–
53	1260	QFM	60	Quenching	1180	QFM	15.0	68	14	0.1	18	1
30				Partially molten powder	1180	QFM	5.0	x	x	x	x	x
51	1260	QFM	45	Cooling	1170	QFM	19.0	64	17	0.1	12	7
54	1260	QFM	45	Quenching	1160	QFM	16.8	x	x	x	23	x
56	1260	QFM	45	Quenching, cooling from 1190 °C with T oscillation	1160	QFM	20.0	46	20	0.1	21	12
27				Partially molten powder	1160	QFM	16.0	x	x	x	x	x
88	1310	QFM	30	Quenching	1150	QFM	13.5	x	x	x	x	x
55	1260	QFM	45	Quenching	1140	QFM	6.5	x	x	x	30	x
52	1260	QFM	60	Cooling	1140	QFM	22.0	39	14	0.1	34	13
63	1290	QFM	30	Cooling	1125	QFM	21.0	30	14	0.1	37	19
105	1335	QFM	60	Quenching, T oscillation	1110	QFM	91.0	4	16	2.2 (Spl)	46	31
165	1360	QFM + 0.8	20	Quenching, T oscillation	1140	QFM + 0.8	17.0	x	x	x	x	x

Table 2 continued

Run#	Starting material conditions			Cooling mode	Final equilibration conditions			Phases identified and proportions				
	T (°C)	fO_2	Duration (min)		T (°C)	fO_2	Duration (h)	Liq (%)	Ol (%)	Cr-spl (%)	Plg (%)	Cpx (%)
166	1360	QFM + 0.8	20	Quenching, T oscillation	1125	QFM + 0.8	14.0	x	x	x	x	x
59	1290	QFM	30	Quenching	1190	QFM + 1.8	10.5	x	x	x	x	–
99	1355	QFM	60	Quenching	1180	QFM + 1.8	12.5	x	x	lot	x	–
58	1290	QFM	45	Quenching, cooling from 1185 °C	1160	QFM + 1.8	12.0	54	15	1.1	20	10

Run conditions and modal abundances from experiments on B62/2 picrite. Cooling paths are shown on the Appendix figure 2. The first 109 experiments were run at the University of Bristol. Experiments 110–185 were run at ETH Zürich

higher Cr# and lower Fe#[4] than in isothermal experiments at the same temperature. The Fe# increases upon cooling (from 0.32 at 1280 °C, to 0.78 at 1110 °C), together with TiO_2 (Fig. 7). Spinel is distinctly more abundant in oxidized experiments (~1 vol%) (Fig. 3e). Conversely, it is rare and corroded in reduced (QFM-2.2) experiments (Fig. 3f) and is absent in clinopyroxene-bearing runs. The Fe^{2+}/Fe^{3+} ratio of spinel is strongly affected by the fO_2, with higher Fe^{3+} content and Fe# under oxidized conditions (Figs. 7a, 8c).

In the basaltic experiments, minor spinel (maximal Cr# = 0.46 at 1150 °C, QFM) saturates at 1160 °C. At 1090 °C, abundant titanomagnetite crystallizes (7 vol%), and the liquid has a ferrogabbro composition (Figs. 2, 7b). Under reduced conditions, Cr-spinel and titanomagnetite coexist.

Spinels in picrite–gabbro and gabbro experiments follow very similar trends. They have a slightly lower Al/(Cr + Al) and higher Fe# than the B62/2 picrite (Fig. 7a) consistent with variation in starting compositions. The gabbro spinel Mg# and Cr# vary within a limited range. Noticeably, the Fe^{3+} does not increase from liquidus to solidus conditions (Fig. 8).

Along the picrite–troctolite QFM liquid line of descent, Cr# increases from 0.11 (Al-spinel) to 0.48 (Cr-spinel) in the interval from 1230 (58 vol% melt) to 1190 °C (28 vol% melt). Concomitantly, the Fe# strongly increases to 0.47 (Figs. 7a, 8). At QFM-1.2, Cr# reaches a maximum value of 0.54 at 1180 °C. At similar temperatures, the TiO_2 concentration is slightly higher in picrite–troctolite experiments compared to picrite experiments, despite the lower Ti content of the starting material, most probably related to a lower melt fraction (Fig. 7b). Spinel in the troctolite-only experiment at 1210 °C (5 vol% liquid) is strongly Al-enriched (Al/[Al + Cr] = 0.98).

In picrite–troctolite experiment reacted for 2 h at 1250 °C, we observe a 200-μm reaction rim with olivine and spinel at the interface between the two magmas (Fig. 9). The spinel modal abundance varies from 1.2 vol% in troctolite to 3.5 vol% in the inner part of the reaction rim to 0.1 vol% in the picrite. The spinel chemistry spatially evolves from Al-spinel in troctolite to Cr-spinel in the picrite. The two extremes in composition are identical to the picrite and troctolite experiments equilibrated under similar conditions (Fig. 8). At the same time, the liquid Al_2O_3 content decreases from 18.4 to 14.2 wt.%, and the Cr_2O_3 concentration increases from 0 to 0.13 wt.%.

Olivine

The olivine proportion in picrite experiments increases from 3 vol% at 1280 °C to ~15 vol% at 1110 °C (Fig. 5). The forsterite (Fo) content varies very little until clinopyroxene

---

[4] Fe# = molar $Fe^{2+}/(Mg + Fe^{2+})$.

Table 3 Gas mixing furnace experiments (1 atm, anhydrous) and run products

Run#	Starting material conditions			Cooling mode	Final equilibration conditions			Phases identified and proportions				
	T (°C)	fO_2	Duration (min)		T (°C)	fO_2	Duration (h)	Liq (%)	Ol (%)	Cr-spl (%)	Plg (%)	Cpx (%)
Experiments with 11JL33 basalt												
176					1230	QFM-1.2	0.5	100	–	–	–	–
167	1235	QFM-1.2	30	Quenching, T oscillation	1170	QFM-1.2	2.5	×	×	–	–	–
168	1235	QFM-1.2	30	Quenching, T oscillation	1150	QFM-1.2	3.5	×	×	–	×	×
169	1235	QFM-1.2	30	Quenching, T oscillation	1135	QFM-1.2	4.3	×	×	–	×	×
151	1210	QFM	20	Quenching, cooling with T oscillation	1125	QFM-1.2	4.3	×	×	×	×	×
170	1235	QFM-1.2	30	Quenching, T oscillation	1120	QFM-1.2	14.0	×	×	–	×	×
171	1235	QFM-1.2	30	Quenching, cooling, T oscillation	1085	QFM-1.2	4.3	×	×	×	×	×
177					1210	QFM-0.7	0.4	100	–	–	–	–
132	1210	QFM-0.7	20	Quenching	1150	QFM-0.7	3.5	×	×	×	×	±
133/2	1210	QFM-0.7	20	Quenching, T oscillation	1135	QFM-0.7	3.5	×	×	×	×	×
133/1	1210	QFM-0.7	20	Quenching	1130	QFM-0.7	3.5	×	×	×	×	×
134	1210	QFM-0.7	20	Quenching, T oscillation	1150	QFM-0.7	3.5	×	×	×	×	×
110					1180	QFM	17.0	100	–	–	–	–
64	1290	QFM	45	Quenching, cooling from 1230 °C	1170	QFM	7.4	100	–	–	–	–
113	1230	QFM	15	Cooling from 1230 °C, T oscillation	1150	QFM	43.0	86	4	<0.1	10	–
70	1290	QFM	30	Quenching, cooling from 1190 °C	1125	QFM	19.1	×	×	<0.1	×	–
124	1215	QFM	0	Cooling from 1215 °C, T oscillation	1120	QFM	20.0	57	6	<0.1	30	7
71	1250	QFM	30	Quenching, T oscillation	1090	QFM	67.3	33	3	7 (Spl)	38	19
129	1200	QFM	15	Cooling with T oscillation	1085	QFM	117.0	×	×	x (Spl)	×	×
130	1200	QFM	20	Quenching, T oscillation	1075	QFM	24.0	×	×	x (Spl)	×	×
131	1210	QFM	20	Quenching, T oscillation	1060	QFM	50.0	2	3	5 (Spl)	53	37

Run conditions and modal abundances from experiments using 11JL33 basalt. Cooling paths are shown on the Appendix figure 2. The first 109 experiments were run at the University of Bristol. Experiments 110–185 were run at ETH Zürich

**Table 4** Gas mixing furnace experiments (1 atm, anhydrous) and run products

Run#	Starting material conditions			Cooling mode	Final equilibration conditions			Phases identified and proportions				
	T (°C)	fO$_2$	Duration (min)		T (°C)	fO$_2$	Duration (h)	Liq (%)	Ol (%)	Cr-spl (%)	Plg (%)	Cpx (%)
Experiments with 50:50 mix of B62/2 picrite + 11JL16 troctolite												
179					1370	QFM-1.2	0.4	96	4	–	–	–
97	1370	QFM	180	Quenching	1200	QFM-1.2	16.3	x	x	x	x	–
149				Partially molten powder	1190	QFM-1.2	43	x	x	x	x	–
146	1370	QFM-1.2	20	Quenching, cooling from 1250 °C, T oscillation	1180	QFM-1.2	48.0	31	24	0.1	45	–
185	1370	QFM-1.2	20	Quenching, T oscillation	1170	QFM-1.2	17	x	x	x	x	x
96					1370	QFM	3.0	100	–	–	–	–
77	1460	air	30	Quenching, T oscillation	1250	QFM	3.3	78	22	0.2	–	–
76	1320	QFM	30	Quenching, T oscillation	1230	QFM	4	69	18	0	13	–
75	1320	QFM	20	Quenching, T oscillation	1210	QFM	7.2	x	x	x	x	–
78	1460	air	15	Quenching, T oscillation	1190	QFM	6.75	x	x	0	x	–
74	1320	QFM	30	Quenching, T oscillation	1190	QFM	12.0	28	32	0.1	40	–
143	1370	QFM	20	Quenching, cooling from 1250 °C with T oscillation	1190	QFM	20.0	x	x	x	x	–
95	1370	QFM	180	Quenching	1185	QFM	15.0	30	x	x	x	–
144	1370	QFM	180	Quenching, cooling from 1260 °C with T oscillation	1180	QFM	44.0	32	28	0.1	40	–
146	1370	QFM	180	Quenching, cooling from 1250 °C with T oscillation	1170	QFM	67.3	x	x	x	x	x
79	1460	air	15	Quenching, T oscillation	1160	QFM	6.6	13	23	1.5	50	12
80	1460	air	15	Quenching, cooling from 1170 °C	1145	QFM	94.0	T < solidus				
180					1400	QFM + 0.8	0.4	100	–	–	–	–
122/1	1360	QFM	60	Quenching, T oscillation	1220	QFM + 0.8	20.0	x	x	x	x	–
122/2				Partially molten powder	1220	QFM + 0.8	20.0	x	x	x	x	–
123	1360	QFM	60	Quenching, T oscillation	1190	QFM + 0.8	1.5	x	x	x	x	–
141	1400	QFM + 0.8	20	Quenching, T oscillation	1190	QFM + 0.8	26.5	x	x	x	x	–
142	1400	QFM + 0.8	20	Quenching, cooling from 1260 °C	1190	QFM + 0.8	73.0	x	x	x	x	–
Experiments with 11JL16 troctolite												
153	1500	QFM-1.2	20	Quenching				100	–	±	–	–
81	1500	air	15	Quenching	1210	QFM	15.3	5	x	x	x	–

Run conditions and modal abundances from experiments using a 50:50 mix of B62/2 picrite +11JL16 troctolite and 11JL16 troctolite. Cooling paths are shown on the Appendix figure 2. The first 109 experiments were run at the University of Bristol. Experiments 110–185 were run at ETH Zürich

Table 5 Gas mixing furnace experiments (1 atm, anhydrous) and run products

Run#	Starting material conditions			Cooling mode	Final equilibration conditions			Phases identified and proportions				
	T (°C)	fO₂	Duration (min)		T (°C)	fO₂	Duration (h)	Liq (%)	Ol (%)	Cr-spl (%)	Plg (%)	Cpx (%)
Experiments with 50:50 mix of B62/2 picrite + 11JL27 gabbro												
173	1360	QFM	20	quenching, T oscillation	1190	QFM-1.2	42.0	x	x	<0.1	x	x
184	1360	QFM-1.2	20	quenching, T oscillation	1160	QFM-1.2	17	x	x	–	x	x
115	1500	QFM	15	Quenching	1290	QFM	1.5	100	–	–	–	–
86	1310	QFM	45	Quenching	1235	QFM	4.1	98	2	0.1	–	–
73	1320	QFM	30	Quenching, T oscillation	1225	QFM	3.8	97	2	0.1	1	–
69	1290	QFM	45	Quenching, cooling from 1250 °C	1210	QFM	5.7	x	x	x	x	–
68	1290	QFM	45	Quenching, cooling from 1230 °C	1190	QFM	8.8	70	9	0	19	2
85	1310	QFM	45	Quenching, T oscillation	1170	QFM	16.75	33	9	0	35	23
116	1500	QFM	15	Quenching, T oscillation	1165	QFM	51.0	x	x	x	x	x
66	1290	QFM	45	Cooling	1140	QFM	10.3	20	7	0.1	42	31
Experiments with 11JL27 gabbro												
181	1350	QFM-1.2	20	Quenching, cooling from 1240 °C, T oscillation	1190	QFM-1.2	15	x	x	x	x	x
182	1350	QFM-1.2	20	Quenching, cooling from 1240 °C, T oscillation	1170	QFM-1.2	37.0	x	x	x	x	x
83	1290	QFM	60	Quenching	1230	QFM	2.0	98	1	0.1	1	–
108	1355	QFM	60	Quenching, cooling from 1240 °C with T oscillation	1210	QFM	15.0	x	x	x	x	x
72	1320	QFM	30	Quenching, T oscillation	1210	QFM	17.5	x	x	x	x	x
94	1295	QFM	55	Quenching, cooling from 1210 °C, T oscillation	1190	QFM	1	30	x	x	x	x
65	1290	QFM	45	Quenching, cooling from 1230 °C	1170	QFM	6.5	25	7	<0.1	48	20

Run conditions and modal abundances from experiments using a 50:50 mix of B62/2 picrite +11JL27 gabbro and 11JL27 gabbro. Cooling paths are shown on the Appendix figure 2. The first 109 experiments were run at the University of Bristol. Experiments 110–185 were run at ETH Zürich
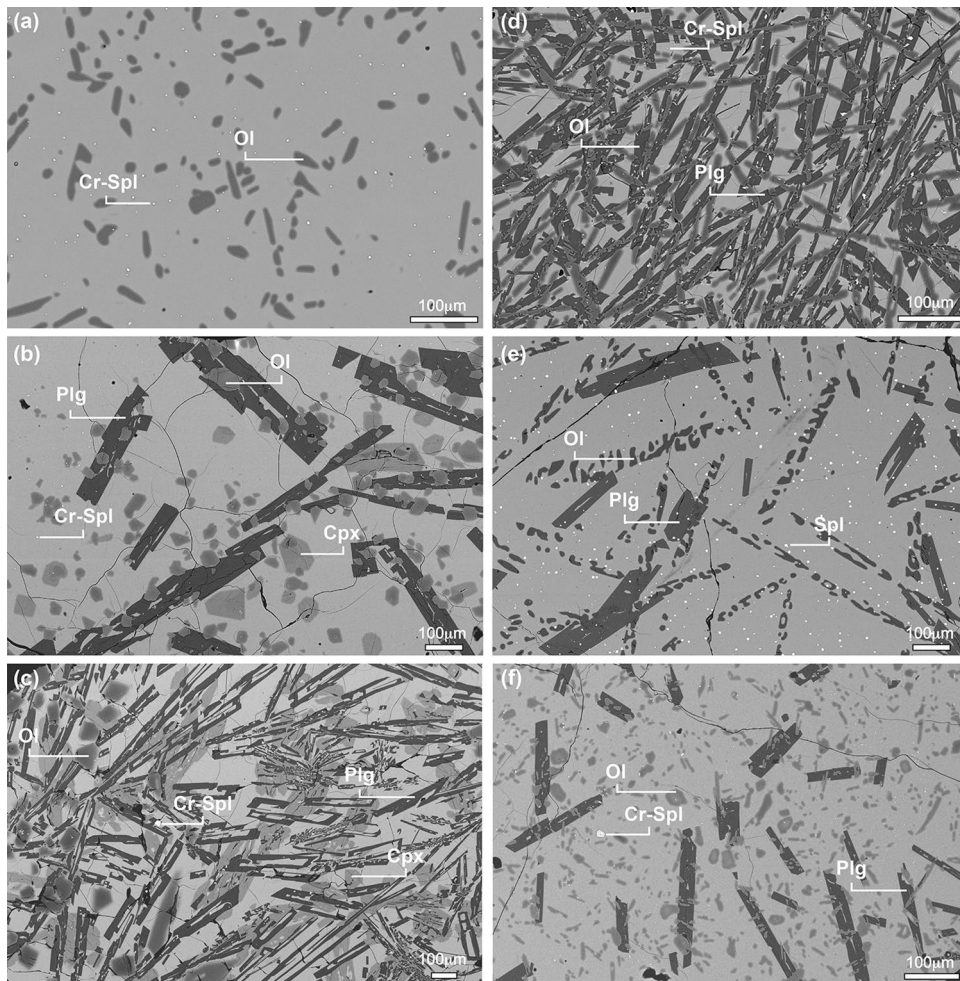
Fig. 3 BSE images of representative experimental run products (see Tables 2, 3, 4, and 5 for conditions). **a** Picrite at 1210 °C, QFM (run#87), illustrating few olivine and Cr-spinel crystals. Spinel grains are ~3 μm in diameter and require high spatial-resolution FEG-EMPA analysis. **b** Picrite at 1170 °C, QFM (run#51), showing the first occurrence of clinopyroxene. **c** Picrite at 1125 °C, QFM (run #63), with 30 vol% glass. Crystallization of large euhedral crystals in figures **b** and **c** was achieved by slow cooling (Heber et al. 2007) and temperature oscillation (Mills et al. 2011; Mills and Glazner 2013). The mineral modes in slowly cooled experiments are indistinguishable from isothermal experiments. Olivine crystals show zoning (especially at low temperature). **d** Picrite–troctolite hybrid (50–50 %) at 1190 °C, QFM (run #78). The melt fraction is lower than in picrite at similar temperatures. Cr-spinel mode is higher than in picrite, and clinopyroxene saturation temperature is lowered to 1170 °C. **e** Picrite at 1180 °C, QFM + 1.8 (run #99). Under more oxidized conditions, spinel mode is enhanced, and its composition is more Fe^{3+}-rich. f) Picrite at 1180 °C, QFM-2.2 (run #61). Under more reducing conditions, spinel is distinctly Fe^{3+}-poor and becomes unstable following clinopyroxene saturation, as evidenced by corroded texture. Abbreviations: *Ol* olivine, *Cr-spl* Cr-spinel, *Spl* spinel, *Plg* plagioclase, *Cpx* clinopyroxene. *Scale bar* is 100 μm

saturation at 1180 °C (Fig. 6). At identical melt volume fraction, Fo is slightly higher in oxidized experiments due to reduction in Fe^{2+}/Fe^{3+} ratio in the coexisting melt. Olivine is zoned in cooling rate experiments, especially when equilibrated at a low final temperature. However, rim composition is identical to olivine crystals in isothermal experiments. In the basaltic experiments, olivine saturates at 1160 °C. The crystals have the lowest forsterite content (down to 0.54).

At identical temperatures, the olivine fraction is lower in picrite–gabbro (50:50 mix) and gabbro experiments (Fig. 3d). Glass in picrite–gabbro and gabbro experiments is relatively Fe-depleted, and the olivine forsterite content is, therefore, elevated compared to picrite experiments. At identical temperatures, the olivine fraction is higher for the picrite–troctolite 50:50 mix (Fig. 3d), but the forsterite and NiO contents are indistinguishable from B62/2 liquids prior to clinopyroxene saturation.

Plagioclase

In the picritic experiments, plagioclase saturates at 1200 °C (85 vol% melt) and modally increases to 45 vol%
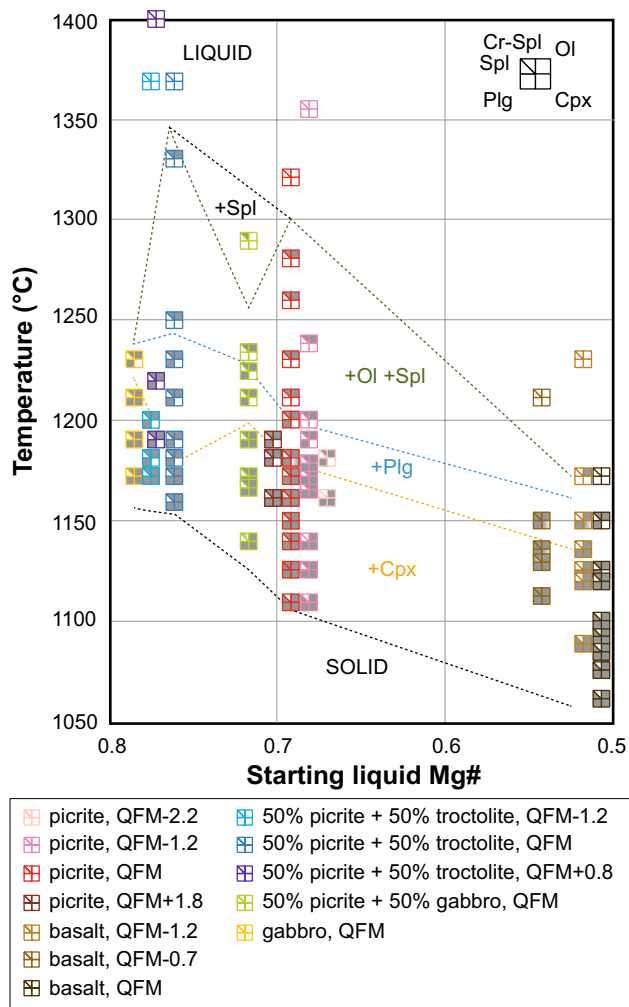
Fig. 4 Schematic representation of equilibrium mineral parageneses (*filled gray fields* in *boxes*) in picrite (B62/2, Upton et al. 2002), basalt, picrite–troctolite, picrite–gabbro, and gabbro experiments (QFM-2.2 to QFM + 1.8) (see Table 1 for starting compositions and Tables 2, 3, 4, and 5 for run conditions and modal abundances), as a function of temperature and Mg# of starting material. Spinel is stable in most experiments. Abbreviations: *Cr-spl* Cr and Al-spinel, *Spl* magnetite and titanomagnetite, *Ol* olivine, *Plg* plagioclase, *Cpx* clinopyroxene

at 1110 °C (4 vol% melt) (Figs. 4, 5). The anorthite content regularly decreases, while the Fe_2O_3 content linearly increases upon cooling at QFM. The fO_2 has no effect on the anorthite content, but plagioclase is more Fe-rich at more oxidized conditions, supporting prevalent incorporation of Fe^{3+} (Wilke and Behrens 1999). Under reducing conditions, the Fe_2O_3 content decreases down temperature. Crystals in cooling rate experiments are unzoned, and their chemistry is identical to plagioclase in isothermal runs.

In the basaltic liquid experiments, plagioclase is a liquidus phase, together with olivine and spinel, at 1160 °C.
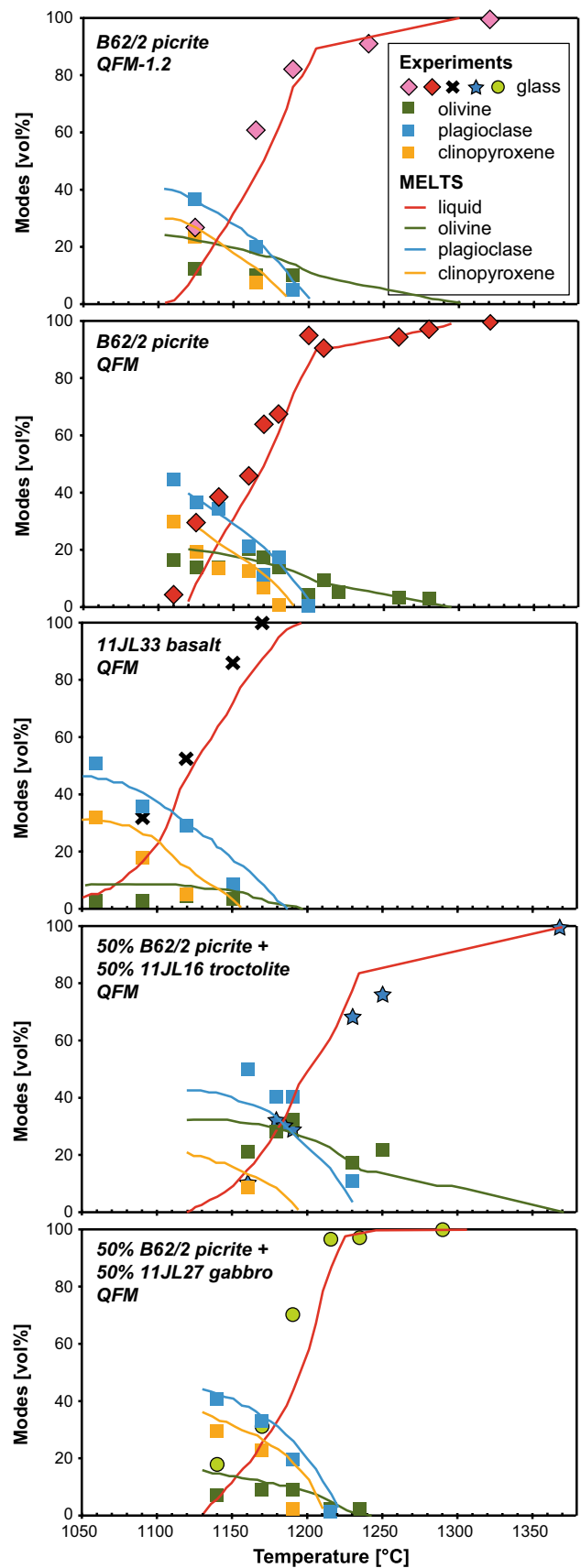
◄ **Fig. 5** Mineral mode (vol%) in 0.1 MPa experiments. The liquid fraction is high until plagioclase fractionation starts and strongly decreases thereafter. Clinopyroxene saturation temperature is systematically lower than plagioclase one. Calculations using the MELTS (Ghiorso and Sack 1995; Asimow and Ghiorso 1998) algorithm at identical conditions show a good correspondence in mineral modes and saturation temperatures. Modal estimates have uncertainties of less than ±5 vol%

The anorthite content extends the picrite plagioclase trend, down to An_{51}. The Fe_2O_3 progressively decreases during cooling, once titanomagnetite saturates.

In picrite–gabbro and gabbro experiments, the plagioclase saturation temperature increases to 1230 and ~1240 °C, respectively. At similar temperature, the plagioclase anorthite content is higher than in pure picrite experiments (Fig. 6). The Fe_2O_3 concentration is lower in hybrid liquid experiments.

In picrite–troctolite experiments, plagioclase saturates at ~1240 °C, and its modal abundance increases rapidly. At 1190 °C (38 vol% melt), it amounts to ~36 vol%. The plagioclase anorthite content is higher than along the B62/2 picrite liquid line of descent (up to An_{86} in picrite–troctolite experiment at 1230 °C) (Fig. 6). The plagioclase Fe_2O_3 content in picrite–troctolite experiments is highly variable.

Clinopyroxene

For the picrite QFM line of descent, clinopyroxene saturates at 1180 °C (68 vol% melt), and its proportion progressively increases to 30 vol% at 1110 °C (Figs. 4, 5). The clinopyroxene Al_2O_3 and Fe_2O_3 concentrations are distinctly higher, and Cr, Fe^{2+}, and Si contents are lower under oxidized conditions (Fig. 6). TiO_2 increases constantly during cooling (not shown), from 0.8 to 2.2 wt.%, regardless of fO_2.

In the basaltic liquid experiments, clinopyroxene saturates from 1120 °C at QFM, but at 1150 °C at QFM-0.7 and QFM-1.2. The Mg# and Cr_2O_3 (<0.3 wt.%) contents are the lowest of all experiments. The Al_2O_3 content shows a large scatter (Fig. 6). TiO_2 increases from 1.1 to 2 wt.% at 1085 °C, before it drops to 0.9 at lower temperature, once titanomagnetite saturates.

In picrite–gabbro and gabbro experiments, the clinopyroxene saturation temperature is increased to ~1200 and ~1220 °C, respectively. The clinopyroxene mode is highest along these liquid lines of descent, and the Cr_2O_3 concentration is distinctly higher (up to 1.40 wt.%) (Fig. 6). As for olivine, the clinopyroxene Mg# is higher than in picrite experiments, and the TiO_2 concentration is distinctly lower (increase from 0.1 to 1.3 wt.%).

In picrite–troctolite experiments, clinopyroxene saturation is delayed until 1170 °C. The Al_2O_3 and Cr_2O_3 concentrations are similar to those in the picrite experiments at QFM.

MELTS calculations

It is instructive to compare our experimental results to those calculated using MELTS (Ghiorso and Sack 1995; Asimow and Ghiorso 1998). MELTS calculations were run using identical starting picritic and basaltic liquid compositions and similar conditions to our experiments. Mineral modes and saturation temperatures appear to accurately reproduce our Rum liquid line of descent (Fig. 5). The spinel, olivine, clinopyroxene, and liquid compositions are also very similar (Figs. 6, 8), but the predicted plagioclase anorthite content is systematically too low; clinopyroxene Cr_2O_3 content is not considered by MELTS (Cr is only incorporated into Cr-spinel). This comparison confirms that MELTS calculations can be used to estimate anhydrous basalt liquid and crystal compositions at low pressure. Hybrid melt experiments' mineral saturation temperatures and modal abundances are also well reproduced by MELTS calculations.

As a first approximation, based on the observation that MELTS calculations are valid at our conditions, we have run additional MELTS calculations varying the pressure (up to 0.3 GPa), starting liquid composition (Rum picritic and basaltic dykes, picrite doped with 0.2 wt.% Cr_2O_3, 50 % plagioclase or 50 % clinopyroxene crystals, troctolite, or gabbro melt), oxygen fugacity (QFM + 0.8 to QFM-2), and varying water content (anhydrous to 0.2 wt.%), while considering both equilibrium and fractional crystallization. The various liquid lines of descent are presented in Fig. 8b. Most calculations were run along a fixed oxygen buffer, which is consistent with the experiments, but not necessarily appropriate to natural systems. It is interesting to note that calculations where the fO_2 is left free to vary during crystallization from initially reduced conditions (QFM-1) produce a second Fe-rich, Si-poor, low-temperature liquid at the saturation point of whitlockite/apatite. Such an immiscible Fe-rich liquid has not been documented on Rum, but has been described from the Skaergaard and Sept Iles layered intrusions (Jakobsen et al. 2005; Charlier et al. 2011) and the British Tertiary Volcanic Province island of Mull (Kerr et al. 1999).

Case study: Cumulates of the Rum Eastern Layered Intrusion

Our experimental results can be used to evaluate magmatic evolution in the Rum Eastern Layered Intrusion. The Rum cumulate assemblage comprises olivine-rich gabbro (60–75 vol% olivine, 15–35 vol% plagioclase, and <15 vol% clinopyroxene), troctolite (15–55 vol% olivine, 45–85 vol% plagioclase, and <10 vol% clinopyroxene), and gabbro (5–20 vol% olivine, 50–60 vol% plagioclase, and 20–50 vol% clinopyroxene) (Holness et al. 2007; Leuthold et al. 2014a). Poikilitic gabbro with
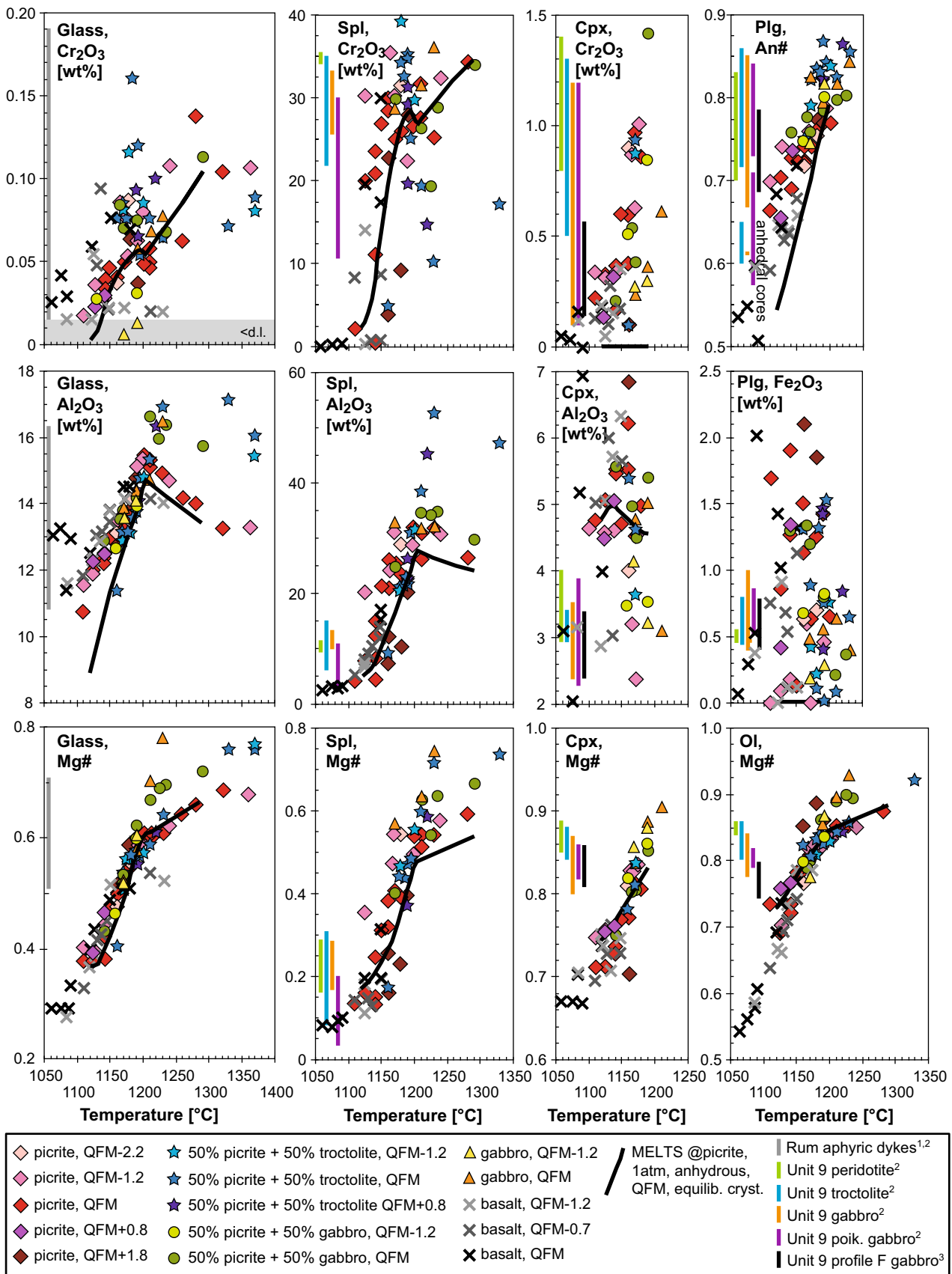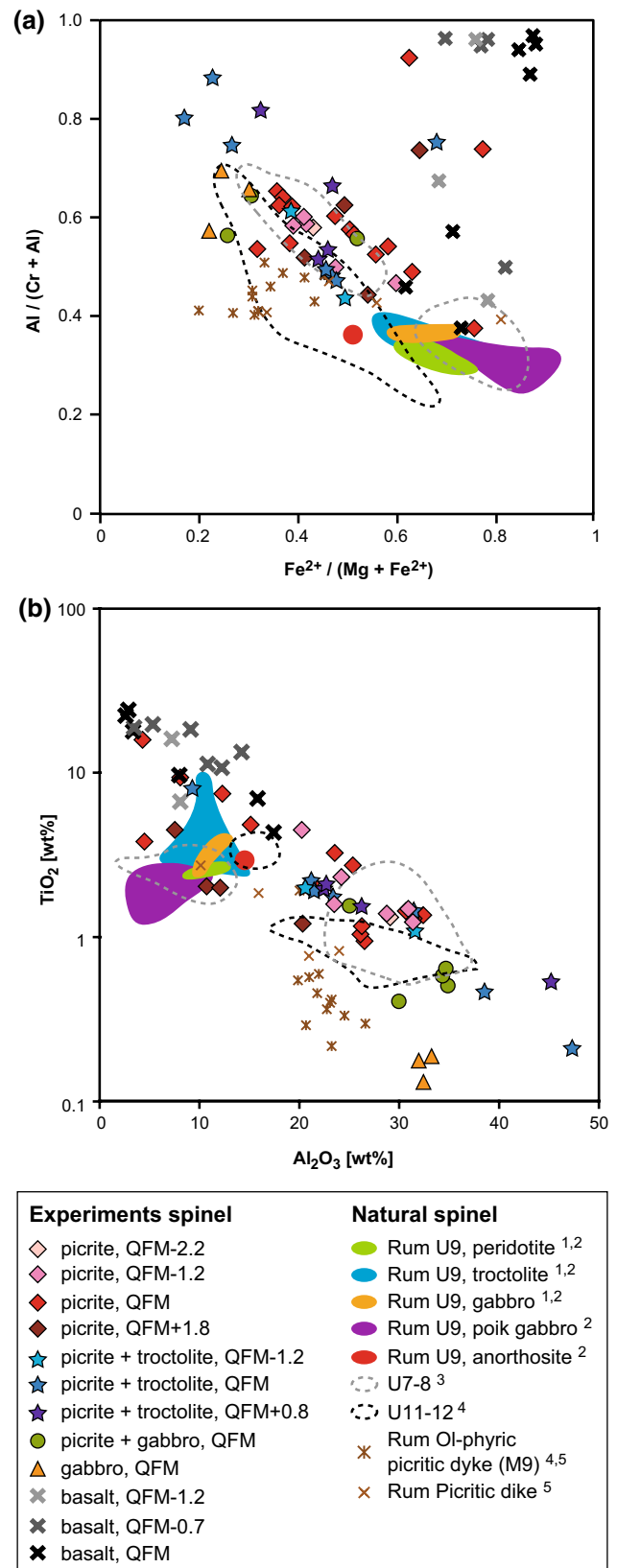
◄**Fig. 6** Glass and mineral chemistry as a function of temperature (averaged compositions). The *vertical bars* indicate the variation in mineral compositions of Rum aphyric dykes and Unit 9 minerals (data from Holness et al. 2007; Leuthold et al. 2014a). Spinel, olivine, and clinopyroxene chemistry is strongly dependent on fO_2. The 11JL33 basalt follows a similar evolution as the B62/2 picrite liquid line of descent, but lacks the most primitive crystals found in the picrite experiments. At identical temperature (i.e., lower melt fractions), the plagioclase anorthite content is higher in picrite–troctolite, picrite–gabbro and gabbro experiments compared to picrite experiments. High-temperature olivine and clinopyroxene (when present) have a higher Mg# in picrite–gabbro and gabbro experiments. [1]McClurg (1982), [2]Leuthold et al. (2014a), [3]Holness et al. (2007)

Fig. 7 Spinel chemistry (averaged compositions). **a** Fe#► (Fe# = Fe^{2+}/[Mg + Fe^{2+}]) progressively increases upon cooling, while Al/(Cr + Al) decreases. The experimental data reveal systematically higher Al/(Cr + Al) than the Rum Unit 9 grains. Spinel chemistry in picrite–troctolite experiments is highly variable in Al/(Cr + Al), ranging from low ratio at high temperature to higher ratio than in picrite experiments at intermediate temperature. Through rapid re-equilibration with olivine down to sub-solidus conditions, spinel becomes Fe^{2+}-rich and Mg-poor (Roeder et al. 1979; Scowen et al. 1991; Kamenetsky et al. 2001, O'Driscoll et al. 2010). **b** Down temperature, spinel becomes Ti-rich. Prior to plagioclase saturation, spinel Al content increases slightly. Spinels crystallized from Ti-poor and Al-rich hybrid melts have lower Ti and higher Al contents than spinels in picrite experiments (at the same melt fraction). [1]Holness et al. (2007), [2]Leuthold et al. (2014b), [3]O'Driscoll et al. (2009), [4]O'Driscoll et al. (2010), [5]Upton et al. (2002)

clinopyroxene oikocrysts and Cr-spinel-bearing anorthosite are also found. Along the profile F (see location on Appendix figure 1) sampled by Holness et al. (2007) across Units 8 and 9, the Unit 9 peridotite sill is absent, and cumulates are mainly composed of texturally mature gabbro with olivine, plagioclase, and clinopyroxene as liquidus phases. These are interpreted to be unmodified by subsequent reactive liquid flow processes (Holness et al. 2007). Leuthold et al. (2014a) studied the Unit 9 in the profile M area, sampled by Sides (2008, unpublished PhD thesis), 400 m south of profile F.

Spinel

At the Unit 7–8 and 11–12 boundaries, millimeter-thick chromitite seams occur at the interface between overlying olivine-rich feldspathic peridotite and underlying feldspar-rich allivalite (anorthosite, troctolite) (Dunham and Wadsworth 1978 and references therein; O'Driscoll et al. 2009b, 2010). Spinel is frequently associated with plagioclase, either in anorthosite or mantled by plagioclase in olivine rim embayments [similar to Bell and Claydon

(a) Plot of Al / (Cr + Al) versus Fe^{2+} / (Mg + Fe^{2+})

(b) Plot of TiO_2 [wt%] versus Al_2O_3 [wt%]

Experiments spinel	Natural spinel
picrite, QFM-2.2	Rum U9, peridotite [1,2]
picrite, QFM-1.2	Rum U9, troctolite [1,2]
picrite, QFM	Rum U9, gabbro [1,2]
picrite, QFM+1.8	Rum U9, poik gabbro [2]
picrite + troctolite, QFM-1.2	Rum U9, anorthosite [2]
picrite + troctolite, QFM	U7-8 [3]
picrite + troctolite, QFM+0.8	U11-12 [4]
picrite + gabbro, QFM	Rum Ol-phyric picritic dyke (M9) [4,5]
gabbro, QFM	Rum Picritic dike [5]
basalt, QFM-1.2	
basalt, QFM-0.7	
basalt, QFM	

Natural crystals
- U9 peridotite [1,2]
- U9 Troctolite [1,2]
- U9 Gabbro [2]
- U9 Poikilitic gabbro [2]
- U9 Anorthosite [2]
- U7-8 (seam + dispersed) [3,4]
- U11-12 (seam + dispersed) [4,5]
- Ol-phyric picritic dyke (M9) [4,6]
- Picritic dike (B62/2) [6]

MELTS calculations
- 1atm, QFM, dry, B62/2 picrite
- 1atm, QFM, dry, B62/2 picrite, solid fractionation
- 1atm, QFM, dry, B62/2 picrite + 0.2wt% Cr_2O_3
- 1atm, QFM+0.8, dry, B62/2 picrite
- 1atm, QFM-2, dry, B62/2 picrite
- 1atm, QFM-2, dry, B62/2 picrite, solid fractionation
- 1atm, fO_2-free (initial QFM-1), dry, B62/2 picrite, solid fractionation
- 0.3GPa, QFM, dry, B62/2 picrite
- 0.3GPa, QFM, 0.2wt% H_2O, B62/2 picrite
- 1atm, QFM, dry, 50% B62/2 picrite + 50% 11JL16 troctolite
- 1atm, QFM-2, dry, 50% B62/2 picrite + 50% 11JL16 troctolite
- 1atm, QFM-2, dry, 50% B62/2 picrite + 50% 11JL16 troctolite, solid fractionation
- 1atm, QFM, dry, 50% B62/2 picrite + 50% 11JL27 gabbro
- 1atm, QFM, dry, 11JL33 basalt

Experiments spinel
- picrite, QFM-2.2, 1180°C
- picrite, QFM-1.2, 1240-1125°C
- picrite, QFM, 1280-1110°C (cooling + equilibrium)
- picrite, QFM+1.8, 1190-1160°C
- 50% picrite + 50% troctolite, QFM-1.2, 1200-1180°C
- 50% picrite + 50% troctolite, QFM, 1330-1160°C
- 50% picrite + 50% troctolite QFM+0.8, 1220-1190°C
- 50% picrite + 50% gabbro, QFM, 1290-1170°C
- gabbro, QFM, 1230-1170°C
- basalt, QFM-1.2, 1125°C
- basalt, QFM-0.7, 1150-1130°C
- basalt, QFM, 1150-1060°C
- picrite-troctolite reaction, QFM-1.2, 1250°C, 2 hours

◀**Fig. 8** Spinel trivalent cations chemistry. **a** Natural spinels from the Rum Eastern Layered Intrusion (Unit 7–8 and 11–12 boundaries, Unit 9 and picritic dykes [M9 and B62/2]) (individual analyses) (modified after Leuthold et al. 2014a and O'Driscoll et al. 2010 and references therein). **b** Calculations using MELTS (Ghiorso and Sack 1995; Asimow and Ghiorso 1998) covering a wide range of P-T-X-fO_2 conditions at which the Rum cumulates may have formed. QFM and oxidized picrite fail to reproduce the Rum Unit 9 Cr-rich spinels. Intermediate temperature spinel crystallized under reduced conditions should have high Cr#. Fractional crystallization, especially under reduced conditions, produces higher Cr# spinel. The Al/(Al + Cr) ratio is lowered when the fO_2 is left free. Spinel crystallizing at moderate pressure or from hydrous melt results in even lower Cr#. Plagioclase-doped picrite (not shown) and picrite-troctolite hybrid melt spinels show a large Al/(Cr + Al) scatter. Fractional crystallization under reduced conditions best reproduces the Unit 9 chromite. High-temperature Cr-rich spinels are absent along the basalt liquid line of descent. **c** Spinel equilibrated at 0.1 MPa from anhydrous picritic liquid variously affected by hybridization with mafic cumulate (gabbro, troctolite) (averaged compositions) (see Table 1 for compositions). Along the picritic liquid line of descent, spinel Al_2O_3 concentration increases up to the point of plagioclase saturation. Upon plagioclase crystallization, spinel Cr# increases until clinopyroxene saturates. With subsequent cooling, spinel rapidly evolves to magnetite and titanomagnetite compositions. Abundant Fe^{3+}-rich spinel crystallizes under oxidized conditions. Conversely, Fe^{3+}-poor spinel is rare under reduced conditions and becomes unstable following clinopyroxene saturation. Gabbro assimilation results in very limited variation in Cr-spinel chemistry during cooling. In contrast, troctolite assimilation strongly modifies spinel chemistry, generating Al-rich spinels at high-temperature, Cr-rich spinel at ~1180 °C, and Fe^{3+}-rich spinels at lower temperature. The Rum Unit 9 chromites are best reproduced by picrite–troctolite experiments at 1180 °C, QFM-1.2. Selected experimental temperatures [°C] are shown for reference. The *dotted blue* line shows the individual spinel analyses across the reaction rim in the picrite-troctolite reaction experiment (run#154) (see Fig. 9 and Appendix table 2). The *beige shaded* areas delimit the Rum Units 7–8 and 11–12 boundaries and Unit 9 spinel compositional fields (see Fig. 8a). [1]Holness et al. (2007), [2]Leuthold et al. (2014a), [3]O'Driscoll et al. (2009), [4]O'Driscoll et al. (2010), [5]Dunham and Wilkinson (1985), [6]Upton et al. (2002)

(1992) for the Skye layered intrusion] (e.g., see Fig. 4e, h in O'Driscoll et al. 2010). Similar textural associations are observed in other layered intrusions (see Lenaz et al. 2011). At the Unit 7–8 boundary (O'Driscoll et al. 2009b), spinel shows two trends, with large Al/(Al + Cr) and Fe^{3+} variations (Fig. 8a). At the Unit 11–12 boundary (O'Driscoll et al. 2010), spinels show limited Fe^{3+} enrichment, but the strongest Al/(Al + Cr) variation.

In Unit 9, the spinel grains are disseminated throughout the cumulates (i.e., mostly peridotite, troctolite, and rare anorthosite). Spinel grains from the Unit 9 matrix (i.e., not fully included in olivine, plagioclase, or clinopyroxene) analyzed by Holness et al. (2007) and Leuthold et al. (2014a) generally have a higher Cr# (0.53–0.03) than grains crystallized along the B62/2 picrite QFM liquid line of descent (0.38–0.06) (Fig. 8). The Cr-spinel Al/(Cr + Al) ratio shows limited variation, and Fe^{3+} strongly increases from anorthosite to peridotite, troctolite, gabbro, and poikilitic gabbro. Spinel grains in most poikilitic gabbros and one troctolite sample have low Mg#, TiO_2, and Cr# contents (Figs. 6, 7, 8). In peridotite, and rarely troctolite,

Al-poor spinel occurs as inclusion in olivine or in olivine-hosted recrystallized melt inclusions, in association with hornblende, orthopyroxene, and aspidolite (Leuthold et al. 2014a). Similar recrystallized melt inclusions have been documented in layered intrusions and oceanic lower crust gabbro (e.g., Irvine 1975; Arai et al. 1997; Spandler et al. 2005; Renna and Tribuzio 2011). Spinel itself hosts recrystallized melt inclusions consisting of olivine, plagioclase, apatite, and Ti-spinel. The Unit 9 spinel Cr# is distinctly higher (up to 0.53 in anorthosite and 0.51 in troctolite); then, the Unit 7–8 and 11–12 boundaries discussed above may have a different petrogenesis, as follows:

Olivine

The Unit 9 profile F olivine composition is Fo_{80-75} (Holness et al. 2007). In the profile M area, where reactive liquid flow processes have been characterized in detail (Leuthold et al. 2014a), the olivine composition varies from Fo_{85} in peridotite to Fo_{84-82} in troctolite, to Fo_{84-81} in gabbro and Fo_{82-79} in poikilitic gabbro.

Plagioclase

The plagioclase anorthite content along profile F varies from An_{79} to An_{69} with normal zoning down to An_{65}. In the area studied by Leuthold et al. (2014a), the plagioclase anorthite content (An_{85-80}) shows very little variation. Along profile F (400 m to the North), it is An_{79-69}, and along profile G (300 m further to the north, above a peridotite lens) (Holness et al. 2007), it is An_{90-80}. The Fe_2O_3 content is 0.60 wt.% for peridotite, troctolite, and gabbro and 0.68 wt.% for poikilitic gabbro (Leuthold et al. 2014a).

Clinopyroxene

In Rum Unit 9, the clinopyroxene composition varies widely (Leuthold et al. 2014a). Whereas Fe–Mg cations were locally re-equilibrated, Cr and Al still record the original clinopyroxene composition obtained during precipitation from the melt (Leuthold et al. 2014a). Clinopyroxene core concentrations of Cr and Al show strong variations throughout the cumulate pile, from peridotite (Mg# = 0.89–0.86, Cr_2O_3 = 1.2–1.1 wt.%, Al_2O_3 = 3.3–3.2 wt.%), to troctolite (Mg# = 0.87–0.85, Cr_2O_3 = 1.2–1 wt.%, Al_2O_3 = 3.7–3.2 wt.%) and gabbro (Mg# = 0.86–0.80, Cr_2O_3 = 1.0–0.2 wt.%, Al_2O_3 = 3.5–2.4 wt.%) consistent with Cr depletion during progressive crystallization. Clinopyroxene rims show strong zoning in peridotite (Mg# = 0.87–0.86, Cr_2O_3 = 0.86–0.85 wt.%, Al_2O_3 = 3.1–2.9 wt.%) and troctolite (Mg# = 0.86–0.84, Cr_2O_3 = 1.0–0.5 wt.%, Al_2O_3 = 3.2–2.7 wt.%) and no distinct zoning in gabbro (Mg# = 0.85–0.80, Cr_2O_3 = 1.0–0.3 wt.%, Al_2O_3 = 3.2-2.4 wt.%). Zoning in poikilitic gabbro is strong

and complex (Mg# varies from 0.85–0.82 in the core to 0.85–0.82 in the rim, Cr_2O_3 varies from 1.2 to 0.1 wt.%, Al_2O_3 varies from 3.7 to 2.3 wt.%, TiO_2 varies from 0.58 to 1.2 wt.%) (see Leuthold et al. 2014a for details). Clinopyroxene analyses from a single rock sampled 6 m below the top of profile F show low Mg# (0.86–0.81), Cr_2O_3 (0.57–0.14 wt.%), and Al_2O_3 (3.2–2.2 wt.%) concentrations (unpublished data).

Discussion

Controls on the stability and chemistry of spinel

Because of the distinctive chemical variation in spinels from Rum and other layered intrusions and the widespread usage of spinel as a petrogenetic indicator, it is informative to use our experiments, in conjunction with published experiments (Murck and Campbell 1986; Roeder and Reynolds 1991), to elucidate the important controls on spinel composition. The key parameters responsible for Cr-spinel chemistry are shown schematically in Fig. 10.

Liquid composition

In order to saturate in Cr-spinel, the parental liquid must be TiO_2-poor (<2.8 wt.%), have a low FeO/MgO ratio (<2.0), and contain more than 200 µg/g (ppm) Cr (Thy 1983). Unlike the other major elements in the spinel structure, Cr acts as a trace element in the parental liquid (Ridley 1977). Allan et al. (1988) proposed that the Cr content of spinels within a given magma has little relationship to host liquid Cr content but instead is indirectly controlled by the host magma Al, Fe^{2+}, and Mg contents. Our Cr-rich (picrite) and Cr-poor (basalt) experiments and MELTS calculations refine that proposal: MELTS calculations show that an increase in the starting liquid Cr_2O_3 results in saturation of Cr-enriched spinel at a higher temperature, but its composition at similar temperatures does not change (an addition of 0.2 wt.% Cr_2O_3 to the starting picrite liquid increases Cr-spinel saturation by 150 °C and Cr# from 0.41 to 0.60). Hill and Roeder (1974) also showed that the spinel liquidus is shifted to higher temperature when Cr_2O_3 is added to the starting material. The spinel saturation in Cr-poor basalt experiments is delayed in comparison with Cr-rich picrite experiments and the basalt liquid line of descent lacks Al-rich spinel. According to Kamenetsky et al. (2001), the spinel Mg# at magmatic conditions is directly linked to the parental melt Mg# and Al_2O_3 content. Murck and Campbell (1986) showed that upon cooling from 1450 to 1150 °C, spinel becomes progressively less Cr-rich. This trend is consistent with our experiments and points to the high-temperature Cr depletion of Cr_2O_3-doped melts close to their liquidus (Fig. 8c).

Liquid composition directly affects mineral saturation temperatures. Our results confirm the observations by Roeder and

Reynolds (1991 and references therein) that plagioclase and clinopyroxene stability plays a major role in determining spinel composition, by controlling liquid Al_2O_3 and Cr_2O_3 contents. In picrite experiments, the crystallization of abundant (up to 30 vol%, Table 2) clinopyroxene, accommodating significant amounts of Cr, effectively depletes the liquid in Cr_2O_3, thus driving the spinel chemistry toward Cr-poor composition. The Cr-spinel crystals with the lowest Al/(Cr + Al) ratio and Fe^{3+} concentration crystallize from plagioclase-rich, clinopyroxene-depleted picrite–troctolite hybrid melt (Fig. 8c). A similar Fe^{3+} enrichment trend would be expected in gabbro hybrid experiments; however, the selected gabbro FeO_{tot} is rather low (5.49 wt.% FeO_{tot}). Hybridization with low-Fe gabbro decreases the liquid Fe content, and spinel remains low in Fe over a large temperature range (Figs. 6, 8c). At high temperature, in low-Fe picrite–gabbro and gabbro experiments, olivine also has a high forsterite content at high temperature. We have run additional MELTS calculations using a picrite doped with 50 % plagioclase as starting composition. The chemistry of Cr-spinel is slightly more Cr-rich along fractional liquid line of descent and slightly less Cr-rich along equilibrium liquid line of descent than for picrite-only calculations. The plagioclase abundance and increased stability balance the melt enrichment in Al_2O_3, resulting in a minor effect on spinel chemistry.

Temperature

The Fe–Mg exchange between spinel and olivine is temperature-sensitive, with Mg preferentially partitioning into olivine with decreasing temperature (Roeder et al. 1979) and has been used as thermometer (e.g., Irvine 1965; Roeder et al. 1979; Engi 1983). Diffusion (discussed below) in the Fe–Mg sites continues at sub-solidus conditions (O'Driscoll et al. 2010). Wilson (1982) concluded that geothermometers based on chromite–silicate equilibria are probably not applicable to slowly cooled layered intrusions, but information on thermal histories may be gleaned from diffusion profiles.

Pressure and water

Spinel is stable from mantle conditions to atmospheric pressure. Dick and Bullen (1984) proposed that Cr solubility in the melt is increased at high pressure. Fisk and Bence (1980) and Roeder and Reynolds (1991) proposed Cr# decreases at higher pressure (at conditions above the plagioclase saturation temperature), accompanied by an increase in Mg# and decrease in Fe^{3+}. Feig et al. (2006) performed oxidized experiments over a wide range of P–T–H_2O conditions on tholeiitic basalts inferring that spinel Cr# decreases as pressure increases from 100 to 200 MPa, followed by a constant value up to 500 MPa. In contrast, Sisson and Grove (1993a, b) showed that in calc-alkaline, high-alumina basalt experiments at NNO, water-saturated

conditions, 1100 °C and 100 MPa, spinel (co-saturated with olivine) has a lower Cr# than at 1050 °C and 200 MPa.

Pressure or water variations have limited effect on spinel composition, but do significantly modify the stability and composition of coexisting plagioclase and clinopyroxene. At higher pressure and/or water content, plagioclase saturation is delayed and clinopyroxene stability increases, resulting in an increased spinel Al/(Cr + Al) ratio. In Feig et al's (2006) experiments, spinel stability increases at high water content (> 3 wt.%), whereas plagioclase stability is decreased. At such conditions, clinopyroxene saturates prior to plagioclase and coexists with Cr-spinel. In this particular case, the water content was directly and positively linked with oxygen fugacity, and thus, spinel in hydrated melts resulted in higher Fe^{3+}, due to H_2 loss. At similar water activities and temperature, spinel in high-pressure experiments is slightly more Fe^{3+}-rich and Cr-poor, because spinel saturation temperature is increased. Thus, low-pressure spinels have the capacity to attain the highest Cr# for a given bulk liquid composition. The Fe# and TiO_2 are only marginally affected by pressure and H_2O variations at a given fO_2.

Oxygen fugacity

Fe^{3+} stabilizes spinel; hence, increasing fO_2 promotes precipitation of abundant Fe^{3+}-rich spinel from basaltic liquids (Hill and Roeder 1974; Ridley 1977; Sharpe and Irvine 1983; Murck and Campbell 1986). Our experiments produce abundant (~1 vol%) Fe^{3+}-rich spinel at QFM + 1.8. In the picrite, picrite–gabbro and gabbro experiments at and above QFM, spinel coexists with olivine, plagioclase, and clinopyroxene over ~40 °C (Fig. 4), until the liquid Cr content is depleted to such an extent that chromite is no longer stable (Irvine 1967). This contrasts with the generally accepted idea that spinel + melt would react to clinopyroxene or to olivine + anorthite via peritectic reactions (Irvine 1967; Hill and Roeder 1974; Roeder 1994) at low pressure (<~0.5 GPa, Grove et al. 1992). This principle is adapted from the haplobasaltic, Cr- and Fe-free forsterite–anorthite–diopside system where the non-ternary, spinel phase ($MgAl_2O_4$) field is terminated at a divergent peritectic point followed down temperature by the forsterite–anorthite cotectic (Morse 1980; Soulard et al. 1994). This system cannot, however, be used to infer phase equilibria between Cr–Al–Fe–Mg spinels and silicate phases where complex solid solutions exist, and the degree of freedom is increased due to at least five additional relevant components (Fe, O, Cr, Ti, and Na) allowing for large stability fields wherein spinel coexists with three or more silicate mineral phases plus melt. Hill and Roeder (1974) showed a gap in spinel crystallization under reduced conditions, where Cr-spinel is replaced by clinopyroxene in a peritectic reaction and only reoccurs at low temperature as Ti-magnetite (or ulvospinel). Our experiments confirm Fe^{3+}-poor spinel occurs

only in trace amounts at QFM-2.2 and temperatures in excess of 1180 °C; it is absent in lower temperature runs.

Differentiation

The 11JL33 basalt represents a fractionated liquid from a parental Rum B62/2 picrite. Crystal chemistry in both liquid lines of descent follows a similar evolution, but basalt experiments lack the most primitive crystals found in the picrite experiments (Figs. 6, 8c). MELTS calculations show that spinels crystallized via equilibrium or fractional crystallization along the QFM liquid line of descent differ little in their composition (Fig. 8b). Spinels obtained in the QFM cooling rate experiments show very limited Cr enrichment compared to isothermal experiments. Conversely, MELTS fractional crystallization calculations performed under reducing conditions produce more Cr-rich spinel than equilibrium crystallization (Fig. 8b). Leaving the oxygen fugacity free in MELTS calculations produces spinel with even higher Cr#, especially for initially reduced conditions.

In plagioclase-saturated experiments, spinels have a slightly lower Al/(Cr + Al) ratio and lower Fe^{3+} in cooling rate experiments (simulating inefficient fractional crystallization) than in isothermal experiments (true equilibrium crystallization). The glass composition is also slightly depleted in Al_2O_3 in cooling rate experiments. The estimated plagioclase modes are not systematically higher in cooling rate experiments, but the anorthite content is. Thus, plagioclase crystallization directly influences spinel chemistry.

Irvine (1975) proposed that increased melt polymerization (NBO/T, e.g., by increased silica content) would decrease the number of octahedral sites in the melt. As Cr cations have a strong preference for octahedral sites (Burns 1975), increased polymerization would significantly reduce Cr-spinel solubility in the melt, promoting early Cr-spinel precipitation. According to Thy (1983), local depletion in melt Cr content is due to crystallization of Cr-spinel, with large spinel/melt partition coefficient for Cr (Hill and Roeder 1974). Such small-scale fractionation may be responsible for grain-to-grain variation in Cr# with relatively constant Al/Fe^{3+} and a lack of correlation with Mg#. Our observations infer that the small proportion of Cr-spinel equilibrium crystallization at high temperature has little effect on the spinel and liquid Cr contents. In contrast, the crystallization of abundant clinopyroxene effectively depletes both the liquid and coexisting spinel in Cr over a small temperature range.

Re-equilibration

Irvine (1980) pointed out that even cumulus grains whose textures do not appear to have been modified may have had their composition changed extensively by reactive liquid flow processes (i.e., post-cumulus metasomatism, as defined by Irvine

1982). In spinels Fe^{2+}–Mg; Cr–Al; Fe^{3+}–Cr, Al; Fe, Ti–Cr, Al cation substitutions take place (Ridley 1977). In the $FeAl_2O_4$-$MgAl_2O_4$ system, intra-spinel and spinel–melt and spinel–olivine Fe^{2+}-Mg diffusion are very fast, whereas spinel–melt Al, Cr, Fe^{3+}, and Ti diffusion rates are slow (Wilson 1982; Ozawa 1984; Scowen et al. 1991; Allan 1994; Roeder et al. 2001; Suzuki et al. 2008). Consequently, sub-solidus reactions only allow Fe–Mg exchanges (O'Driscoll et al. 2010). At near- and sub-solidus conditions, spinel Mg# is controlled by the rate of cooling and re-equilibration with silicates (Kamenetsky et al. 2001). Hoshide and Obata (2014) showed Cr-spinel Fe^{3+} enrichment, with very limited Cr^{3+} enrichment, when re-equilibrated with evolved interstitial melt. Significant diffusion can occur through and within olivine and modify spinel inclusion compositions (Scowen et al. 1991; Hoshide and Obata 2014), which should not therefore be used as indicators of original liquidus compositions. Diffusion through plagioclase is slower, and the chemistry of spinel inclusions is less modified as a consequence (Hoshide and Obata 2014).

Bell and Claydon (1992) proposed that Al-rich Cr-spinel reacts with Ca-rich melt to produce plagioclase, olivine, and Cr-rich spinel, accompanied by a decrease in Mg# and increase in TiO_2. This peritectic reaction explains the increased amounts of intercumulus plagioclase and the small amounts of intercumulus olivine associated with the more chromian spinel present in layered intrusions (e.g., O'Driscoll et al. 2009b). More Ti-rich, Al-poor Rum spinel equilibrated over a long period of time at a low temperature with intercumulus melt (O'Driscoll et al. 2010; Lenaz et al. 2011). O'Driscoll et al. (2010) indicate the importance of the modal proportion of spinel in buffering the reaction: the more abundant it is, the less the re-equilibration.

Petrogenesis of Cr-spinel in the Rum Eastern Layered Intrusion

Unit 7–8 and 11–12 boundary Al-spinel seams

Rum spinel petrogenesis has long been discussed. Henderson and Suddaby (1971), Henderson (1975), Putnis and Price (1979), and Henderson and Wood (1981) have shown that seam spinels are much more Al-rich and Cr-poor and have a lower Fe# than spinels in the nearby plagioclase-rich rock and overlying peridotite. Chromite Al enrichment can result from the reaction with olivine and either plagioclase or from a melt rich in plagioclase component, a reaction known as the "Rum trend" (Barnes and Roeder 2001 after Henderson 1975). Fe^{3+} enrichment, on the other hand, is interpreted as progressive crystallization or reaction with evolved interstitial liquid (Henderson 1975; O'Driscoll et al. 2010). Young (1984) suggested that in Unit 7 evolved, interstitial basaltic liquid migrated upward from the troctolite and anorthosite crystal mush,

blended with newly injected picrite, and created a hybrid magma saturated with Cr-spinel (i.e., the model of Irvine 1977). For Dunham and Wadsworth (1978), the occurrence of the Unit 11–12 chromitite bands within a zone whose mineralogy shows rapid changes from Fe–Na to Mg–Ca-rich minerals (i.e., a reverse of the normal magmatic trend) reflects the influx of new Mg-rich magma into the system. In particular, Dunham and Wadsworth (1978) suggest that the Mg- and Al-rich spinel had crystallized directly from the picrite, without subsequent reaction with the crystal mush or interstitial liquid. O'Driscoll et al. (2009b, 2010) showed that the chemistry of Cr-spinel at the boundary between Units 7 and 8 evolved toward a low Al concentration prior to a progressive Fe^{3+} enrichment at constant Cr# (Fig. 8). They proposed a model whereby Cr-spinel crystallized in situ, from a hybrid melt produced by assimilation of troctolite cumulate into infiltrating reactive picritic liquid, one of the processes simulated in our experimental study.

Following Irvine (1977), Roeder and Reynolds (1991) proposed that mixing of a hot, plagioclase-undersaturated primitive magma, with a plagioclase-enriched magma, could produce hybrid melts that crystallize chromite with low and highly variable Cr#. Magma mixing and dissolution of plagioclase could also have been responsible for the so-called alumina Rum trend described above. Following these ideas, O'Driscoll et al. (2009b, 2010) proposed a model whereby abundant picritic liquid (i.e., a mafic olivine-saturated liquid) percolated and assimilated troctolite cumulate to produce a plagioclase-saturated melt. The hybrid melt then crystallized Cr-spinel seams (~2 mm thick) and anorthosite (~10–70 cm thick). Our experiments show 50:50 % mixing of picrite and troctolite liquids produces a hybrid melt that crystallizes Al-rich spinel and olivine at liquidus temperature, thereafter fractionating abundant plagioclase (~An_{86}) from 1240 °C and saturating in clinopyroxene at 1160 °C. The Al/(Cr + Al) ratio of high-temperature Al-spinel decreases dramatically upon cooling, reaching the highest measured Cr# of 0.54 at 1180 °C at QFM-1.2, before it quickly evolves toward Fe^{3+}-rich composition (Fig. 8c). The Units 7–8 and 11–12 Al-rich spinel seams (Al/[Cr + Al] as high as 0.70) are therefore consistent with crystallization from picrite–troctolite hybrid liquid, as suggested by O'Driscoll et al. (2009b, 2010), at a temperature close to 1210 °C and QFM condition. This temperature is higher than that determined for natural grains utilizing the olivine–spinel exchange thermometer of Ballhaus et al. (1991) and Princivalle et al. (1999) (see O'Driscoll et al. 2009b; Lenaz et al. 2011), a fact we attribute to re-equilibration during cooling.

In our experiments, the Al- and Cr-spinel modal proportions are low (typically 0.1–0.2 vol%), and the crystallization of a 2-mm-thick seam with 30 vol% spinel requires

effective sorting and settling of denser spinel from a 30- to 60-cm-thick magma layer, in agreement with field observations. Spinel extraction from a basaltic liquid appears to be very efficient (Manoochehri and Schmidt 2014). At ~1230 to ~1180 °C, the liquid fraction amounts to 60–30 vol% in picrite–troctolite hybrid magma, allowing dense crystals to settle out as long as they are not part of a touching framework. This model could explain the formation of the main spinel seam, at the interface between peridotite (picrite) and anorthosite/troctolite.

Subsidiary spinel seams are sandwiched between overlying peridotite and troctolite. Spinel often occurs in indentations and embayment structures in olivine oikocrysts (see Fig. 3 in O'Driscoll et al. (2009b). In our reaction experiments, we have tested the effect of chemical disequilibrium between picrite and troctolite melt at constant temperature, pressure, and oxygen fugacity. Through picrite liquid hybridization with troctolite partial melt, the glass and the spinel Al and Cr compositions vary considerably, and the spinel modal abundance increases markedly (up to 3.5 vol%; Fig. 9). Despite the low oxygen fugacity, the spinel proportion is the highest we have measured. These observations corroborate the model of spinel seam formation during picrite–troctolite melt hybridization. Subsequent plagioclase fractionation increases the spinel Cr#. It is curious to note abundant Cr-spinel crystallized in the picrite–troctolite reaction zone, where plagioclase is absent. We hypothesize that picritic liquid percolated into the troctolite crystal mush and dissolved plagioclase, which is unstable at 1250 °C. The melt Al content increased, stabilizing spinel that crystallized between relict olivine

grains. As the picrite Cr content is high and spinel is the only phase incorporating Cr into its structure, Al- and Cr-rich spinel crystallizes. The Cr-rich picrite and Al-rich troctolite melt ratio is crucial here. Based on the observation that the spinel composition in reaction experiments spans the range of spinel crystallized from equilibrium experiments, we suggest that spinel with higher Cr# crystallized at lower temperature (upon cooling or during reaction at lower temperature). However, evidence for reaction seems to disappear over prolonged reaction time. Additionally, spinel is modally more abundant on the troctolite side of the reaction rim, at ca. 100 μm from the picrite contact. This observation supports in situ spinel subsidiary seams crystallization as opposed to gravitational settling of dense spinel. Upon cooling, the hybrid melt will fractionate abundant plagioclase, forming the anorthosite.

Unit 9 Cr-spinel

We established earlier that distinct physicochemical parameters can increase the spinel Cr# of a single magma, approaching those found in Rum Unit 9 (Fig. 10): (1) Low water content increases plagioclase stability and Al depletion; (2) low pressure reduces clinopyroxene stability and Cr extraction and also raises the melt and spinel Cr content, at sub-liquidus condition; (3) spinel Cr_2O_3 concentrations are higher under low fO_2 conditions, but its modal abundance is strongly reduced. The corroded texture observed at intermediate temperature (1180 °C, QFM-2.2) indicates a peritectic reaction with the liquid and clinopyroxene. Crystallization of abundant chromite cannot be explained by
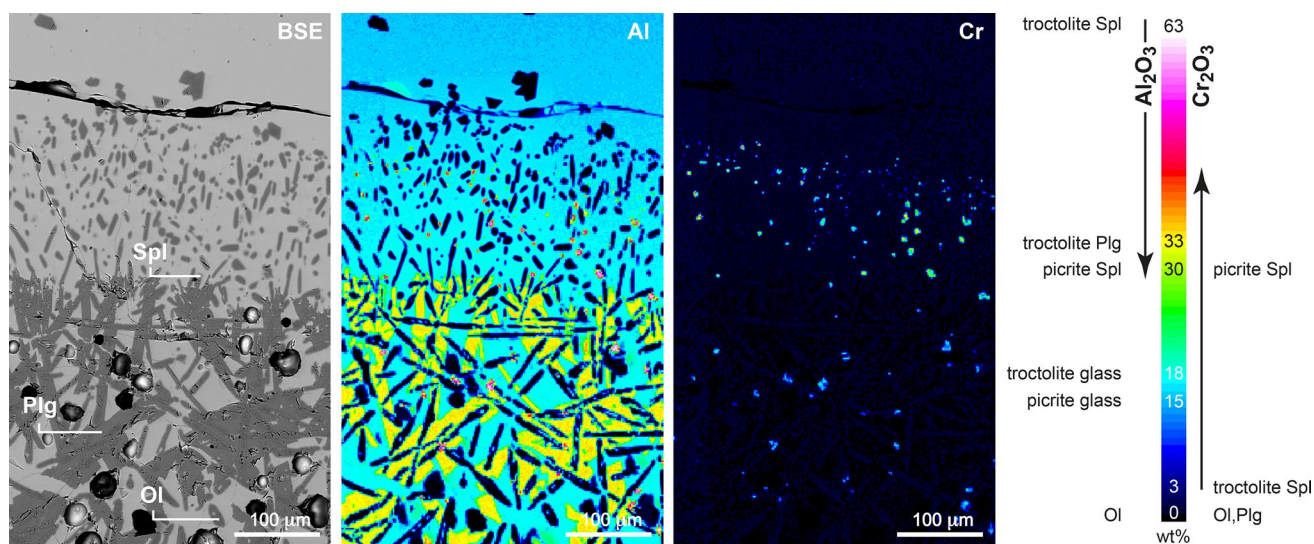
Fig. 9 BSE image and Al and Cr X-ray maps of the interface between a synthetic picrite and a troctolite initially equilibrated at 1250 °C and QFM-1.2, left to react for 2 h at similar conditions (run #154). Note the high abundance of Al- and Cr-spinel (up to 3.5 vol%) in the troctolite side of the hybrid reaction zone, where plagioclase is absent
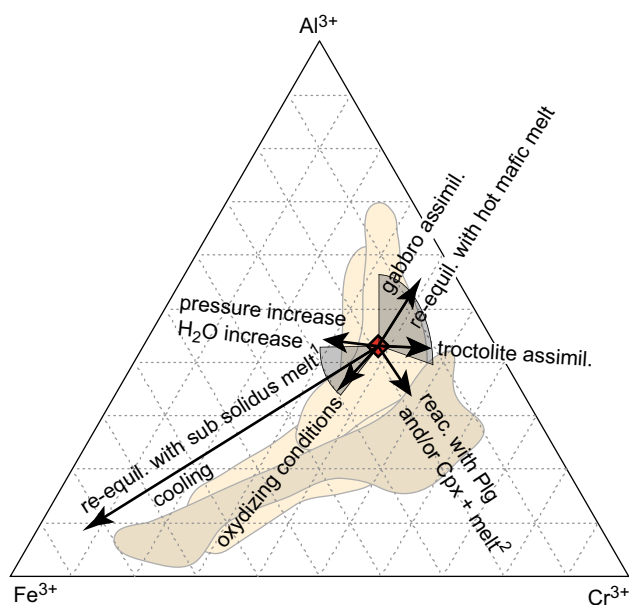
Fig. 10 Schematic diagram illustrating potential modification of Cr-spinel chemistry by common magmatic processes. The diamond symbol indicates the Cr-spinel composition crystallized from B62/2 picrite starting material at 1180 °C, QFM. The arrows show isothermal chemistry modifications and will change according to different temperatures (e.g., hot mafic, intermediate or cool differentiated interstitial melt). See text for discussions and references. The *beige shaded* areas delimit the Rum Units 7–8 and 11–12 boundaries and Unit 9 spinel compositional fields (see Fig. 8a). [1]Henderson (1975), [2]Bell and Claydon (1992)

low $f\mathrm{O}_2$ conditions alone, unless crystallized over a small temperature interval from a very large magma body or from a clinopyroxene-depleted magma; (4) fractional crystallization has a strong effect on the spinel Cr enrichment at low $f\mathrm{O}_2$, but spinel becomes unstable at low temperature under reduced conditions; and (5) spinel Cr# increases through re-equilibration with plagioclase + melt or clinopyroxene + melt (Wilson 1982; Bédard and Hébert 1998).

High Cr# and Ti and low Mg# and Al-spinel, with a composition very close to the Unit 9 Cr-rich spinel (Figs. 7, 8), crystallize from picrite–troctolite hybrid melt at QFM-1.2, 1180 °C. Clinopyroxene saturation is delayed in picrite–troctolite hybrid experiments, permitting the crystallization of high Cr# spinel even under reduced conditions. Spinels obtained by MELTS fractionation calculations and from the cooling rate experiments have a higher Cr# than those from MELTS equilibrium calculations and from isothermal experiments, respectively. Olivine and plagioclase fractionation could further drive the spinel chemistry toward the Unit 9 chromite composition. Also, higher Cr# spinel crystallizes from MELTS calculations where the $f\mathrm{O}_2$ is allowed to vary (especially for initially reduced conditions). Those two processes were not investigated during our experiments and may account for the minor differences

between experimental and natural crystals. Fe–Mg diffusion occurs down to sub-solidus conditions (O'Driscoll et al. 2010) and may have lowered the Unit 9 spinel Mg# (Roeder et al. 1979; Scowen et al. 1991; Kamenetsky et al. 2001). We propose the Unit 9 Cr-spinels fractionated over a limited temperature range (ca. 1180 °C), from a reduced picrite–troctolite hybrid melt fractionating olivine + plagioclase. These spinels subsequently experienced sub-solidus re-equilibration with olivine.

Unit 9 and 7–8 boundary Fe^{3+}-rich spinel

Spinel crystals in picrite and basalt cooling rate experiments at QFM, ~1125 °C and QFM + 1.8, ~1180 °C have a similar composition to the troctolite, gabbro, and poikilitic gabbro Fe^{3+}- and Ti-rich crystals suggestive of crystallization at such conditions. Alternatively, equilibration of isolated Cr-spinel with evolved interstitial melt would likewise increase the spinel Fe^{3+} content observed in those lithologies (Henderson 1975; Hoshide and Obata 2014). O'Driscoll et al. (2010) inferred that the extent of spinel textural and chemical re-equilibration is inversely proportional to the spinel modal abundance. Thus, re-equilibration of low modal proportions of Cr-spinel with trapped melt (crystallizing abundant Fe-poor plagioclase; Lenaz et al. 2011) could induce strong Fe^{3+} enrichment. Fe^{3+}-rich spinel indeed occurs in the least compacted cumulates (i.e., gabbro and poikilitic gabbro) (Leuthold et al. 2014a). Ridley (1977) suggested an extensive solid solution between Cr + Al and Ti + Fe spinels. Rum Cr-spinel grains show post-cumulus Cr and Al increase and Fe and Ti decrease toward the contact with ilmenite crystals (not shown), possibly produced by spinel oxidation down to ~600 °C (Putnis and Price 1979; O'Driscoll et al. 2010). Finally, Bell and Claydon (1992) proposed that the spinel grains may have been modified by post-cumulus peritectic reaction of Al-rich spinel with melt producing low Mg# and Cr-, Fe^{2+}-, Fe^{3+}-, Ti-rich spinel + plagioclase + olivine. This trend is similar to that in our picrite experiments. Ultimately, in order to explain the Unit 9 titanomagnetite petrogenesis, it is difficult to distinguish between (1) crystallization from a differentiated liquid at QFM or more oxidized conditions, or (2) re-equilibration with a differentiated melt. Both processes overlap when interstitial melt is not efficiently extracted.

M9 picrite accumulated spinel

Spinel in the olivine–phyric and spinel–phyric picritic dyke M9 (Upton et al. 2002; O'Driscoll et al. 2010) has low Ti, Cr#, and $Fe^{2+}/(Mg + Fe^{2+})$ in comparison with the Unit 9 grains (Fig. 7). Upton et al. (2002) suggested the M9 olivine and spinel primocrysts formed at high pressure in a

near-Moho reservoir from a high MgO melt (~20 wt.%) (Upton et al. 2002), prior to remobilization by picritic liquid (~13 wt.% MgO) and emplacement into the Rum Eastern Layered Intrusion. MELTS calculations of picrite at high pressure (0.3 GPa) predict that spinel crystallized at sub-liquidus temperature from a Cr-rich liquid, or under reduced conditions, has a high Cr# similar to natural grains (Fig. 8). The melt Cr_2O_3 content determines the Cr# of the first spinel to saturate, directly influencing the saturation temperature. Looking at Fig. 8b, c, spinel Cr# is high at very high temperature, prior to Al increase. Thus, M9 spinel primocrysts may have crystallized at very high temperature and lower crustal pressure from a more mafic melt than the Unit 9 crystals (i.e., less TiO_2 and FeO and more MgO and Cr_2O_3; Fisk and Bence 1980) prior to emplacement. It is probable that a few Unit 9 spinels were inherited from an M9-type dyke and then re-equilibrated during hybridization with partially molten mafic crystal mushes.

Petrogenesis of the Rum Unit 9 cumulates

Using our picrite and basalt experiments together with the large dataset of natural crystals compositions (Holness et al. 2007; Leuthold et al. 2014a), we attempt to determine the physicochemical conditions for the formation of the Rum Unit 9 cumulates. In Appendix Table 3, we present correspondences based on the Fig. 6. We will first compare the natural grains with the Rum picrite and basalt equilibrium liquid lines of descent. Leuthold et al. (2014a) proposed the phase abundance, saturation temperature, and chemistry were shifted from the equilibrium liquid line of descent though *reactive liquid flow* (Fig. 1). We then test the hypothesis that the Unit 9 cumulates were modified by gabbro and/or troctolite assimilation. It is believed that cumulates in the profile F area (see Appendix figure 1), where the discordant peridotite sill is absent, were not modified by late-stage crystal–melt reactions, thus still showing the original composition.

Olivine

Olivines in profile F are distinctly more fayalitic (Fo_{82-74}) than along other Unit 9 profiles E, G, H, and I (Fo_{87-80}) sampled by Holness et al. (2007). Although we cannot exclude the possibility that the Rum olivine composition was not fully re-equilibrated, the olivine compositions obtained in the picrite (for all fO_2 conditions), picrite–gabbro, and picrite–troctolite experiments overlap with the range of Unit 9 crystals overlying peridotite sills (Fig. 6). Olivine in basalt experiments is more Fe-rich, consistent with the down temperature extension of the picrite experiments. Thus, profile F olivines are consistent with low-temperature picrite and/or hot basalt parental liquids.

Plagioclase

Plagioclase in Rum Unit 9 shows lateral chemical variability, ranging from An_{85-80} in the area studied by Leuthold et al. (2014a) to An_{79-69} 400 m to the north, along profile F of Holness et al. (2007) and An_{90-80} along profile G 300 m further north. While the chemistry of profile F crystals is well reproduced by picrite experiments and corresponds to the range from the point of plagioclase saturation to the solidus, the high anorthite content of Leuthold et al. (2014a) and profile G (Holness et al. 2007) can only be reproduced by hybrid experiments. Alternatively, crystallization from a water-bearing magma would lower the plagioclase liquidus temperature and crystallize plagioclases that are higher in An content (Kuritani 1998). With 0.5 wt.% dissolved water, MELTS calculations show the plagioclase saturation temperature is lowered (~30 °C, co-saturating with clinopyroxene) and the anorthite content is ~4 mol% higher. This is insufficient to explain the most anorthite-rich crystals in Unit 9. MELTS calculations at the maximal estimated crystallization pressure of 50 MPa (Holness 1999) reveal little effect on the anorthite composition compared to 0.001 MPa. Along a fractional crystallization liquid line of descent, the anorthite content would become even lower (e.g., Toplis and Carroll 1995). Anhedral cores, also described by Young (1984) and O'Driscoll et al. (2009b) in the Unit 7, are An_{68-58}, similarly to the 11JL33 basaltic dyke experiments. Anhedral sodic cores certainly crystallized from a basaltic parental magma or from a fractionating dry picritic liquid.

The Unit 9 plagioclase Fe_2O_3 content varies from 0.4 to 0.8 wt.%, with no distinction between core, rim, and anhedral core (profiles F and G in Holness et al. 2007; Leuthold et al. 2014a). In picrite and basalt experiments, plagioclase Fe_2O_3 increases from ~0.6 to ~1.8 wt.% at QFM and is <0.7 wt.% under more reduced conditions. Plagioclase crystallized from hybrid experiments has Fe_2O_3 concentration ranging from 0 to 1.5 wt.%.

Clinopyroxene

The Mg# of cumulate crystals (0.89–0.80 in the profile M area, ~0.86–0.79 along profile F) is higher than those in experiments, except for the high-temperature, reduced picrite, picrite–gabbro, and gabbro experiments. According to Leuthold et al. (2014a), divalent cations were frequently partly re-equilibrated (at least within the individual grains) but trivalent cations were unmodified. The Cr_2O_3 concentration of the experimental clinopyroxene overlaps with the clinopyroxene core composition from all lithologies, except for the Cr_2O_3-poor basalt experiments. Profile F clinopyroxene has low Cr contents identical to basalt, low-temperature picrite and low-temperature reduced picrite-gabbro or

gabbro experiments. Only clinopyroxene crystallized from reduced experiments at high temperature (picrite, basalt, picrite–gabbro, gabbro, and picrite-troctolite) has low Al_2O_3, close to natural Unit 9 grains in the profile M area.

Synthesis

Comparing olivine, plagioclase, and clinopyroxene to experimental crystals shows the Unit 9 profile F gabbro crystallized from a hot (~1160 °C) and dry melt with a composition intermediate between the studied picrite and basalt starting materials. Alternatively, we can not exclude crystallization from a reduced picrite-gabbro or gabbro melt close to its solidus, but there is no obvious field evidence for crystallization from such a melt. Clinopyroxene cores, An-poor plagioclase, and olivine in profiles M, G, H, E possibly crystallized from a hot (~1180 °C), reduced (~QFM-1.2) picrite. Lateral variations may be explained by local accumulation of high-temperature crystals and the segregation of interstitial melt that will fractionate down temperature. Also, gravity currents (Emeleus et al. 1996; Tepley and Davidson 2003; O'Driscoll et al. 2007) may transport and juxtapose grains crystallized under different conditions.

Crystallization along the picrite or basalt liquid lines of descent fails to reproduce the Cr-rich spinel chemistry, the plagioclase high anorthite content and the complex clinopyroxene microtextures in the profile M area. Subsequent to hot reactive picrite intrusion, the chemistry and composition of the overlying cumulative rocks was modified during *reactive liquid flow*. Where low-degree gabbro partial melting was achieved (a few decameters from the sill, according to Leuthold et al. 2014a), a second clinopyroxene generation crystallized around preexisting, partially resorbed crystals, from a reduced gabbro melt at ~1170 °C. Where porosity was sufficient for picritic melt to percolate, the new clinopyroxene generation could alternatively have crystallized from a reduced picrite-gabbro hybrid melt, leading to the formation of complex poikilitic gabbro with clinopyroxene oikocrysts in a troctolitic matrix. Closer to the peridotite sill, the troctolite cumulate high-An, low Fe_2O_3 plagioclase, the low clinopyroxene abundance and the Cr-spinel chemistry all indicate crystallization from a reduced hybrid picrite–troctolite melt. Our experiments highlight an increased melting proportion of plagioclase versus clinopyroxene towards the peridotite sill. Based on successive crystallization–dissolution stages in clinopyroxene microtextures, Leuthold et al. (2014a) were able to demonstrate consecutive partial melting episodes. This suggests most clinopyroxene close to the hot intrusive sill was melted and expelled, leaving a troctolite restite. The latter was intruded and partially melted by a second hot picrite intrusion (see Fig. 16 in Leuthold et al. 2014a). Spinel, An-rich plagioclase, and sparse clinopyroxene crystallized from

this later, hot, reduced hybrid picrite–troctolite melt at 1190 to 1160 °C. Exact temperature estimates may vary slightly (±20 °C), when considering different picrite–gabbro and picrite–troctolite proportions and/or fractional crystallization.

Conclusions

We have determined the Rum parental magma liquid line of descent over a wide range of oxygen fugacity, from liquidus to solidus conditions. The plagioclase saturation temperature is only slightly higher than that of clinopyroxene. We observe excellent agreement with MELTS calculations (Ghiorso and Sack 1995; Asimow and Ghiorso 1998) in terms of crystal saturation temperatures and modal abundances increasing confidence in this algorithm for understanding Rum petrogenesis. The temperatures and modes used in the reactive liquid flow model by Leuthold et al. (2014a) are thus corroborated. Using the plagioclase and clinopyroxene chemistry in Unit 9 and in experiments, we propose that the Rum parental magma was slightly reduced (around QFM-1.2).

We have studied experimentally the effect of mafic cumulate (gabbro and troctolite) melting by cogenetic picrite liquid and melts hybridization. The liquidus and solidus temperatures are shifted from the picrite liquid line of descent in hybrid experiments, in accordance with the cumulate equilibrium temperature. Mineral modes are strongly modified. The plagioclase fraction, in particular, is increased significantly. Assimilation of mafic crystals by mafic melt has a minor, but distinct, effect on the chemistry of the new crystal generation. High-temperature troctolite assimilation decreases spinel Fe#, Cr#, and TiO_2 concentrations. This is best explained by olivine and plagioclase dissolution, releasing MgO and Al_2O_3 to the hybrid melt. Down temperature, abundant plagioclase crystallization strongly depletes the residual melt in Al_2O_3, driving the spinel toward low Al/(Cr + Al). Clinopyroxene removes Cr_2O_3 from the melt, but its stability is reduced in such compositions, favouring crystallization of high Cr# spinel. Chromites from Rum Unit 9 are best explained by troctolite assimilation into invading reactive picrite and crystallization from a hybrid melt. Clinopyroxene and plagioclase compositions cannot be explained simply by crystallization from pure picrite or basalt liquid and also require hybridization with various proportions of gabbro and/or troctolite. Our observations confirm the model of Cr- and Al-spinel precipitation from a hybrid picrite–troctolite melt, proposed by O'Driscoll et al. (2009b, 2010), and Leuthold et al. (2014a). Our combination of natural observations and experiments allowed us to determine the crystallization temperature and parental melt chemistry of the complex Rum Eastern Layered Intrusion cumulates. Our quantitative study demonstrates the importance of considering crystal-melt reactions in intrusive complexes.

References

Allan JF (1994) Cr-spinel in depleted basalts from the Lau Basin back-arc: petrogenetic history from Mg-Fe crystal-liquid exchange. In: Hawkins J, Parson L, Allan J et al (eds) Proc. ODP, Sci. Results, 135. Ocean Drilling Program, College Station, TX, pp 565–584

Allan JF, Sack RO, Batiza R (1988) Cr-rich spinels as petrogenetic indicators: MORB-type lavas from the Lamont seamont chain, eastern Pacific. Am Mineral 73:741–753

Annen C, Blundy JD, Sparks RSJ (2006) The genesis of intermediate and silicic magmas in deep crustal hot zones. J Petrol 47(3):505–539

Arai S, Matsukage K, Isode E, Vysotskiy S (1997) Concentration of incompatible elements in oceanic mantle: effect of melt/wall interaction in stagnant or failed melt conduits within peridotite. Geochim Cosmochim Acta 61(3):671–675

Asimow PD, Ghiorso MS (1998) Algorithmic modifications extending MELTS to calculate subsolidus phase relations. Am Mineral 83:1127–1132

Ballhaus C, Berry RF, Green DH (1991) High pressure experimental calibration of the olivine-orthopyroxene-spinel oxygen geobarometer: implications for the oxidation state of the upper mantle. Contrib Mineral Petrol 107:27–40

Barnes SJ, Roeder PL (2001) The range of spinel compositions in the terrestrial mafic and ultramafic rocks. J Petrol 42(12):2279–2302

Bédard J, Hébert R (1998) Formation of chromitites by assimilation of crustal pyroxenites and gabbros into peridotitic intrusions: north Arm Mountain massif, Bay of Islands ophiolite, Newfoundland, Canada. J Geophys Res 103(B3):5165–5184

Bédard JH, Sparks RSJ, Renner R, Cheadle MJ, Hallworth MA (1988) Peridotite sills and metasomatic gabbros in the Eastern Layered Series of the Rhum complex. J Geol Soc London 145:207–224

Bell BR, Claydon RV (1992) The cumulus and post-cumulus evolution of chrome-spinels in ultrabasic layered intrusions: evidence from the Cuillin Igneous Complex, Isle of Skye, Scotland. Contrib Mineral Petrol 112:242–253

Bell BR, Williamson IT (2002) Tertiary igneous activity. In: Trewin NH (ed) The geology of Scotland, 4th edn. Geol Soc London, London, pp 371–408

Brown GM (1956) The layered ultrabasic rocks of Rhum, Inner Hebrides. Philos T R Soc B 240:1–68

Burns RG (1975) Crystal field effects in chromium and its partitioning in the mantle. Geochem Cosmochim Acta 39:857–864

Cameron EN, Desborough GA (1969) Occurrence and characteristics of chromite deposits—eastern Bushveld Complex. Econ Geol Mon 4:23–40

Campbell IH, Murck BW (1993) Petrology of the G and H chromitite zones in the Mountain View area of the Stillwater Complex, Montana. J Petrol 34(2):291–316

Charlier B, Namur O, Toplis MJ, Schiano P, Cluzel N, Higgins MD, Vander Auwera J (2011) Large-scale silicate liquid immiscibility during differentiation of tholeiitic basalt to granite and the origin of the Daly gap. Geology 39:907–910

Dick HJB, Bullen T (1984) Chromium spinel as a petrogenetic indicator in abyssal and alpine-type peridotites and spatially associated lavas. Contrib Mineral Petrol 86:54–76

Dungan MA, Davidson J (2004) Partial assimilative recycling of the mafic plutonic roots of arc volcanoes: an example from the Chilean Andes. Geology 32(9):773–776

Dunham AC, Wadsworth WJ (1978) Cryptic variation in the Rhum layered intrusion. Mineral Mag 42:347–356

Dunham AC, Wilkinson FCF (1985) Sulphide droplets and the Unit 11/12 chromite nand, Rhum: a mineralogical study. Geol Mag 122(5):539–548

Emeleus CH (1997) Geology of Rum and the adjacent islands. Memoir of the British Geological Survey, Sheet 60 (Scotland)

Emeleus CH (2004) Rum solid geology map 1:20000. Scottish Natural Heritage

Emeleus CH, Gyopari MC (1992) British Tertiary Volcanic Province. Chapman & Hall, London

Emeleus CH, Cheadle MJ, Hunter RH, Upton BGJ, Wadsworth WJ (1996) The Rum Layered Suite. In: Cawthrorn RG (ed) Layered intrusions. Elsevier Science BV, pp 403–439

Engi M (1983) Equilibria involving Al-Cr spinel: Mg-Fe exchange with olivine. Experiments, thermodynamic analysis, and consequences for geothermometry. Am J Sci 283A:29–71

Feig ST, Koepke J, Snow JE (2006) Effect of water on tholeiitic basalt phase equilibria: an experimental study under oxidizing conditions. Contrib Mineral Petrol 152:611–638

Fisk MR, Bence AE (1980) Experimental crystallization of chrome spinel in famous basalt 527-1-1. Earth Planet Sci 48:111–123

Ghiorso MS, Sack RO (1995) Chemical mass transfer in magmatic processes IV. A revised and internally consistent thermodynamic model for the interpolation and extrapolation of liquid–solid equilibria in magmatic systems at elevated temperatures and pressures. Contrib Mineral Petrol 119:197–212

Grieco G, Ferrario A, Mathez EA (2004) The effect of metasomatism on the Cr-PGE mineralization in the Finero Complex, Ivrea Zone, Southern Alps. Ore Geol Rev 24:299–314

Grove TL (1993) Corrections to expressions for calculating mineral components in "Origin of Calc-Alkaline Series Lavas at Medicine Lake Volcano by Fractionation, Assimilation and Mixing" and "Experimental Petrology of normal MORB near the Kane Fracture Zone: 22o-25oN, mid-Atlantic ridge". Contrib Mineral Petrol 114:422–424

Grove TL, Kinzler RJ, Bryan WB (1992) Fractionation of Mid-Ocean Ridge Basalt (MORB). In: Morgan JP, Blackman DK, Sinton JM (eds) Mantle flow and melt generation at Mid-Ocean Ridges. Geophys Monograph 71: 281–310. American Geophysical Union, Washington, DC

Hamilton MA, Pearson DG, Thompson RN, Kelly SP, Emeleus CH (1998) Rapid eruption of Skye lavas inferred from precise U-Pb and Ar-Ar dating of the Rum and Cuillin plutonic complexes. Nature 394:260–263

Heber VS, Brooker RA, Kelley SP, Wood BJ (2007) Crystal-melt partitioning of noble gases (helium, neon, argon, krypton, and xenon) for olivine and clinopyroxene. Geochim Cosmochim Acta 71:1041–1061

Hémond C, Arndt NT, Lichtenstein U, Hofman AW (1993) The heterogeneous Iceland plume: Nd-Sr-O isotopes and trace element constraints. J Geophys Res 98(B9):15833–15850

Henderson P (1975) Reaction trends shown by chrome-spinels of the Rhum layered intrusion. Geochim Cosmochim Acta 39:1035–1044

Henderson P, Suddaby P (1971) The nature and origin of the chrome-spinel of the Rhum Layered Intrusion. Contrib Mineral Petrol 33:21–31

Henderson P, Wood RJ (1981) Reaction relationships of chrome-spinels in igneous rocks—further evidence from the Layered Intrusions of Rhum and Mull, Inner Hebrides, Scotland. Contrib Mineral Petrol 78:225–229

Hildreth W, Moorbath S (1988) Crustal contributions to arc magmatism in the Andes of Central Chile. Contrib Mineral Petrol 98:455–489

Hill R, Roeder P (1974) The crystallization of spinel from basaltic liquid as a function of Oxygen fugacity. J Geol 82(6):709–729

Holness MB (1999) Contact metamorphism and anatexis of Torridonian arkose by minor intrusions of the Rum Igneous Complex, Inner Hebrides, Scotland. Geol Mag 136:527–542

Holness MB, Winpenny B (2009) The Unit 12 Allivalite, Eastern Layered Intrusion, Isle of Rum: a textural and geochemical study of an open-system magma chamber. Geol Mag 146(3):437–450

Holness MB, Hallworth MA, Woods A, Sides RE (2007) Infiltration Metasomatism of Cumulates by Intrusive Magma Replenishment: the Wavy Horizon, Isle of Rum, Scotland. J Petrol 48(3):563–587

Hoshide T, Obata M (2014) Spinel inclusions in olivine and plagioclase crystals in a layered gabbro: a marker and a tracer for primary phenocrysts in a differentiating magma reservoir. Contrib Mineral Petrol 168:1049

Irvine TN (1965) Chromian spinel as a petrogenetic indicator. Part 1. Theory. Can J Earth Sci 2:648–672

Irvine TN (1967) Chromian spinel as a petrogenetic indicator. Part 2. Petrologic applications. Can J Earth Sci 4:71–103

Irvine TN (1975) Crystallization sequences in the Muskox intrusion and other layered intrusions—II. Origin of chromitite layers and similar deposits of the magmatic ores. Geochim Cosmochim Ac 39:991–1020

Irvine TN (1977) Origin of chromite layers in the Muskox intrusion and other stratiform intrusions: a new perspective. Geology 5:273–277

Irvine TN (1980) Magmatic infiltration metasomatism, double-diffusive fractional crystallization, and adcumulus growth in the Muskox intrusion and other layered intrusions. In: Hagraves RB (ed) Physics of magmatic processes. Princeton University Press, New Jersey, pp 325–383

Irvine TN (1982) Terminology for layered intrusions. J Petrol 23(2):127–162

Jakobsen JK, Veksler IV, Tegner C, Brooks CK (2005) Immiscible iron- and silica-rich melts in basalt petrogenesis documented in the Skaergaard intrusion. Geology 33:885–888

Kamenetsky VS, Crawford AJ, Meffre S (2001) Factors controlling chemistry of magmatic spinel: an empirical study of associated olivine, Cr-spinel and melt inclusions fro primitive rocks. J Petrol 42(4):655–671

Kent RW (1995) Magnesian basalts from the Hebrides, Scotland: chemical composition and relationship to the Iceland plume. J Geol Soc 152:979–983

Kerr AC, Kent RW, Thomson BA, Seedhouse JK, Donaldson CH (1999) Geochemical evolution of the Tertiary Mull volcano, western Scotland. J Petrol 40:873–908

Kress VC, Carmichael ISE (1991) The compressibility of silicate liquids containing Fe_2O_3 and the effect of composition, temperature, oxygen fugacity and pressure on their redox state. Contrib Mineral Petrol 108:82–92

Kuritani T (1998) Boundary layer crystallization in a basaltic magma chamber: evidence from Rishiri volcano, northern Japan. J Petrol 39(9):1619–1640

Latypov R, O'Driscoll B, Lavrenchuk A (2013) Towards a model for the in situ origin of PGE reefs in layered intrusions: insights from chromitites seams of the Rum Eastern Layered Intrusion, Scotland. Contrib Mineral Petrol 166:309–327

Lenaz D, O'Driscoll B, Princivalle F (2011) Petrogenesis of the anorthosite-chromitite association: crystal-chemical and petrological insights from the Rum Layered Suite, NW Scotland. Contrib Mineral Petrol 162:1201–1213

Leuthold J, Müntener O, Baumgartner LP, Putlitz B, Ovtcharova M, Schaltegger U (2012) Time resolved construction of a bimodal laccolith (Torres del Paine, Patagonia). Earth Planet Sci Let 325–326:85–92

Leuthold J, Blundy JD, Holness MB, Sides R (2014a) Successive episodes of reactive liquid flow through a layered intrusion (Unit 9, Rum Eastern Layered Intrusion, Scotland). Contrib Mineral Petrol 167:1021

Leuthold J, Müntener O, Baumgartner LP, Putlitz B (2014b) Petrological constraints on the recycling of mafic crystal mushes and intrusion of braided sills in the Torres del Paine mafic complex (Patagonia). J Petrol 55(5):917–949

Lipin BR (1993) Pressure increase, the formation of chromite seams, and the development of the ultramafic serie in the Stillwater Complex, Montana. J Petrol 34(5):955–976

Manoochehri S, Schmidt MW (2014) Settling and compaction of chromite cumulates employing a centrifuging piston cylinder and application to layered mafic intrusions. Contrib Mineral Petrol 168:1091

McClurg J (1982) Geology and structure of the northern part of the Rhum ultrabasic complex. University of Edinburgh, PhD thesis (unpublished)

McDonald JA (1965) Liquid immiscibility as one factor in chromitite seam formation in the Bushveld Igneous Complex. Econ Geol Bull Soc 60:1674–1685

Mills RD, Glazner AF (2013) Experimental study on the effect of temperature cycling on coarsening of plagioclase and olivine in an alkali basalt. Contrib Mineral Petrol 166:97–111

Mills RD, Ratner JJ, Glazner AF (2011) Experimental evidence for crystal coarsening and fabric development during temperature cycling. Geology 39:1139–1142

Morse SA (1980) Basalts and phase diagrams: an introduction to the quantitative use of phase diagrams in igneous petrology. Springer, New York, p 493

Murck BW, Campbell IH (1986) The effects of temperature, oxygen fugacity and melt composition on the behaviour of chromium in basic and ultrabasic melts. Geochim Cosmochim Acta 50:1871–1887

Naldrett AJ, Wilson A, Kinnaird J, Yudovkaya M, Chunnett G (2012) The origin of chromitites and related PGE mineralization in the Bushveld Complex: new mineralogical and petrological constraints. Miner Deposita 47:209–232

O'Driscoll B, Hargraves RB, Emeleus CH, Troll VR, Donaldson CH, Reavy RJ (2007) Magmatic lineations inferred from anisotropy of magmatic susceptibility fabrics in Units 8, 9, and 10 of the Rum Eastern Layered Series, NW Scotland. Lithos 98:27–44

O'Driscoll B, Day JMD, Daly JS, Walker RJ, McDonough WF (2009a) Rhenium-osmium isotopes and platinum-group elements in the Rum Layered Suite, Scotland: implications for the Cr-spinel seam formation and the composition of the Iceland mantle anomaly. Earth Planet Sci Let 286:41–51

O'Driscoll B, Emeleus CH, Donaldson CH, Daly JS (2010) Cr-spinel seam petrogenesis in the Rum layered suite, NW Scotland: cumulate assimilation and in situ crystallization in a deforming crystal mush. J Petrol 51(6):1171–1201

O'Hara MJ, Herzberg C (2002) Interpretation of trace element and isotope features of basalts: relevance of field relations,

petrology, major element data, phase equilibria, and magma chamber modeling in basalt petrogenesis: Geochem. Cosmochem Acta 66:2167–2191

O'Driscoll B, Donaldson CH, Daly JS, Emeleus CH (2009b) The roles of melt infiltration and cumulate assimilation in the formation of anorthosite and a Cr-Spl seam in the Rum Eastern Layered Intrusion, NW Scotland. Lithos 111:6–20

Ozawa K (1984) Olivine-spinel geospeedometry: analysis of diffusion-controlled Mg-Fe^{2+} exchange. Geochim Cosmochim Ac 48:2597–2611

Palacz ZA, Tait SR (1985) Isotopic and geochemical investigation of Unit 10 from the Eastern Layered Series of the Rhum intrusion. Northwest Scotland. Geol Mag 122(5):485–490

Power MR, Duncan P, Andersen JCØ, Wheeler PD (2000) Testing the validity of chrome spinel chemistry as a provenance and petrogenetic indicator. Geology 28:1027–1030

Princivalle F, Della Giusta A, De Min A, Piccirillo EM (1999) Crystal chemistry and significance of cation ordering in Mg-Al rich spinels from high grade hornfels (Predazzo-Monzoni, NE Italy). Mineral Mag 63:257–262

Putnis A, Price GD (1979) The nature and significance of exsolved phases in some chrome spinels from the Rhum layered intrusion. Mineral Mag 43:519–526

Renna MR, Tribuzio R (2011) Olivine-rich troctolites from Ligurian ophiolites (Italy): evidence for impregnation of replacive mantle conduits by MORB-type melts. J Petrol 52(9):1763–1790

Renner R, Palacz Z (1987) Basaltic replenishment of the Rhum magma chamber: evidence from unit 14. J Geol Soc London 144:961–970

Ridley WI (1977) The crystallization trends of spinels in the Tertiary basalts from Rhum and Muck and their petrogenetic significance. Contrib Mineral Petrol 64:243–255

Roeder PL (1994) Chromite: from the fiery rain of chondrules to the Kilauea Iki lava lake. Can Mineral 32:729–746

Roeder PL, Reynolds I (1991) Crystallization of chromite and chromium solubility in basaltic melts. J Petrol 32(5):909–934

Roeder PL, Campbell IH, Jamieson HE (1979) A re-evaluation of the olivine-spinel geothermometer. Contrib Mineral Petrol 68:325–334

Roeder PL, Poustovetov A, Oskarsson N (2001) Growth forms and composition of chromian spinel in MORB magma: diffusion-controlled crystallization of chomian spinel. Can Mineral 39:397–416

Saint Blanquat M, Horsman E, Habert G, Morgan S, Vanderhaeghe O, Law R, Tikoff B (2011) Multiscale magmatic cyclicity, duration of pluton construction, and the paradoxical relationship between tectonism and plutonism in continental arcs. Tectonophysics 500:20–33

Saunders AD, Fitton JG, Kerr AC, Norry MJ, Kent RW (1997) The North Atlantic igneous province. In: Mahoney JJ, Coffin MF (eds) Large igneous provinces: continental, oceanic, and planetary flood volcanism. American Geophysical Union, Washington, pp 45–93

Saunders K, Buse B, Kilburn MR, Kearns S, Blundy J (2014) Nanoscale characterisation of crystal zoning. Chem Geol 364:20–32

Scowen PAH, Roeder PL, Helz RT (1991) Reequilibration of chomite within Kilauea Iki lava lake, Hawaii. Contrib Mineral Petrol 107:8–20

Sharpe MR, Irvine TN (1983) Melting relations of two Bushveld chilled margin rocks and implications for the origin of chromitite. Carnegie Inst Wash Yearb 82:295–300

Sisson TW, Grove TL (1993a) Experimental investigations of the role of H$_2$O in calc-alkaline differentiation and subduction zone magmatism. Contrib Mineral Petrol 113:143–166

Sisson TW, Grove TL (1993b) Temperatures and H$_2$O contents of low-MgO high-alumina basalts. Contrib Mineral Petrol 113:167–184

Solano JMS, Jackson MD, Sparks RSJ, Blundy JD, Annen C (2012) Melt segregation in deep crustal hot zones: a mechanism for chemical differentiation, crustal assimilation and the formation of evolved magmas. J Petrol 53(10):1999–2026

Soulard H, Boivin P, Libourel G (1994) Liquid-forsterite-anorthite-spinel assemblage at 1 bar in the CMAS system: implications for low-pressure evolution of high-Al and high-Mg magmas. Eur J Mineral 6(5):633–646

Spandler C, Mavrogenes J, Arculus R (2005) Origin of chromitites in layered intrusions: evidence from chromite-hosted melt inclusions from the stillwater complex. Geology 33(11):892–896

Suzuki AM, Yasuda A, Ozawa K (2008) Cr and Al diffusion in chromite spiel: experimental determination and its implication for diffusion creep. Phys Chem Minerals 35:433–445

Tepley FJ, Davidson JP (2003) Mineral-scale Sr-isotope constraints on magma evolution and chamber dynamics in the Rum layered intrusion, Scotland. Contrib Mineral Petrol 145:628–641

Thy P (1983) Spinel minerals in transitional and alkali basaltic glasses from Iceland. Contrib Mineral Petrol 83:141–149

Thy P, Lesher CE, Nielsen TFD, Brooks CK (2006) Experimental constraints on the Skaergaard liquid line of descent. Lithos 92:154–180

Toplis MJ, Carroll MR (1995) An experimental study of the influence of oxygen fugacity on Fe-Ti oxide stability, phase relations, and mineral-melt equilibria in ferro-basaltic systems. J Petrol 36:1137–1170

Tronnes RG (1990) Basaltic melt evolution of the Hengill Volcanic System, SW Iceland, and evidence for clinopyroxene assimilation in primitive tholeiitic magmas. J Geophy Res 95(B10):15893–15910

Ulmer GC (1969) Experimental investigations of chromite spinels. Econ Geol Monogr 4:114–131

Upton BGJ, Skovgaard AC, McClurg J, Kirstein L, Cheadle M, Emeleus CH, Wadsworth WJ, Fallick AE (2002) Picritic magmas and the Rum ultramafic complex, Scotland. Geol Mag 139:437–452

Wilke M, Behrens H (1999) The dependence of the partitioning of iron and europium between plagioclase and hydrous tonalitic melt on oxygen fugacity. Contrib Mineral Petrol 137:102–114

Wilson AH (1982) The geology of the Great 'Dyke', Zimbabwe: the ultramafic rocks. J Petrol 23(2):240–292

Young IM (1984) Mixing of supernatant and interstitial fluids in the Rhum layered intrusion. Mineral Mag 48:345–350